





Review

Single-Atom Catalysts: A Review of Synthesis Strategies and Their Potential for Biofuel Production

Nurul Asikin-Mijan ^{1,*}, Haslinda Mohd Sidek ², Abdulkareem G. AlSultan ³, Nurul Ahtirah Azman ¹, Nur Ahtirah Adzahar ² and Hwai Chyuan Ong ^{4,5,*}

¹ Department of Chemical Sciences, Faculty of Science and Technology, Universiti Kebangsaan Malaysia (UKM Bangi), Bangi 43600, Selangor, Malaysia; A171032@siswa.ukm.edu.my

² Catalysis Science and Technology Research Centre (PutraCat), Faculty of Science, Universiti Putra Malaysia (UPM Serdang), Serdang 43400, Selangor, Malaysia; lindasidek89@gmail.com (H.M.S.); ahtirahadzahar22@gmail.com (N.A.A.)

³ Department of Chemical and Environmental Engineering, Universiti Putra Malaysia (UPM Serdang), Serdang 43400, Selangor, Malaysia; kream.alsultan@yahoo.com

⁴ Future Technology Research Center, National Yunlin University of Science and Technology, 123 University Road, Section 3, Douliou 64002, Taiwan

⁵ Centre for Green Technology, Faculty of Engineering and Information Technology, University of Technology Sydney, Sydney, NSW 2007, Australia

* Correspondence: nurul.asikin@ukm.edu.my (N.A.-M.); ong1983@yahoo.com (H.C.O.)



Citation: Asikin-Mijan, N.; Mohd Sidek, H.; AlSultan, A.G.; Azman, N.A.; Adzahar, N.A.; Ong, H.C. Single-Atom Catalysts: A Review of Synthesis Strategies and Their Potential for Biofuel Production. *Catalysts* **2021**, *11*, 1470. <https://doi.org/10.3390/catal11121470>

Academic Editors: José María Encinar Martín and Sergio Nogales Delgado

Received: 30 October 2021

Accepted: 28 November 2021

Published: 30 November 2021

Publisher's Note: MDPI stays neutral with regard to jurisdictional claims in published maps and institutional affiliations.



Copyright: © 2021 by the authors. Licensee MDPI, Basel, Switzerland. This article is an open access article distributed under the terms and conditions of the Creative Commons Attribution (CC BY) license (<https://creativecommons.org/licenses/by/4.0/>).

Abstract: Biofuels have been derived from various feedstocks by using thermochemical or biochemical procedures. In order to synthesise liquid and gas biofuel efficiently, single-atom catalysts (SACs) and single-atom alloys (SAAs) have been used in the reaction to promote it. SACs are made up of single metal atoms that are anchored or confined to a suitable support to keep them stable, while SAAs are materials generated by bi- and multi-metallic complexes, where one of these metals is atomically distributed in such a material. The structure of SACs and SAAs influences their catalytic performance. The challenge to practically using SACs in biofuel production is to design SACs and SAAs that are stable and able to operate efficiently during reaction. Hence, the present study reviews the system and configuration of SACs and SAAs, stabilisation strategies such as mutual metal support interaction and geometric coordination, and the synthesis strategies. This paper aims to provide useful and informative knowledge about the current synthesis strategies of SACs and SAAs for future development in the field of biofuel production.

Keywords: biofuel; single-atom catalyst; surface chemistry; alternative fuel

1. Introduction

Biofuel is a fuel derived from biomass. Biofuels include bio-char, ethanol, biodiesel, biogas, biohydrogen, and biosynthetic gas fuels [1,2]. The need for more biofuel production is owed to the continued anthropogenic emission of greenhouse gases (GHGs) by fossil fuel consumption coupled with the quickly dwindling availability of fossil fuels. By utilising distinctive thermochemical or biochemical procedures, biofuel can be created from various types of feedstocks, for example, food crops, farming waste, modern waste, waste cooking oils, and animal fats. Thermochemical techniques involve the conversion of biomass to biofuel via pyrolysis or gasification processes [3], while biochemical processes involve the conversion of biomass into sugar via enzymatic or chemical hydrolysis using an acid approach, where the sugar is applied to microbial fermentation to obtain biofuel [4]. Biofuels are generally classified as being first-, second-, third-, or fourth-generation. They are characterised by their sources of biomass. First-generation biofuels are typically produced from food sources (i.e., sugarcane, vegetable oils, and grains) [5], while second-generation biofuels are derived from inedible biomass such as non-food crops, solid waste, and energy crops (i.e., woody biomass and wheat straw) [6]. In the case of third-generation

biofuels, these fuels involve utilising algal feedstock [7], while fourth-generation biofuels are produced from genetically modified microorganisms, specifically cyanobacteria and algae [8]. It is noteworthy to mention that the majority of the biofuel produced today comes from the first generation of feedstock or from food crops. For example, the United States and Brazil use corn and sugarcane, whereas European nations use wheat and grain for ethanol creation [9]. As of late, critical concerns have been raised about first-generation biofuel production because of the food versus fuel issue. Therefore, specialists have been urged to investigate different routes for biofuel production. As a result, the focus is on second-generation biofuels [5]. Overall, lignocellulose feedstock is largely responsible for producing second-generation biofuels. Lignocellulose is a substance composed of one aromatic polymer (lignin) and two carbohydrate polymers (cellulose and hemicellulose). These substances can be obtained from raw biomass, waste biomass obtained from agriculture, and energy crops specifically grown for biofuel production [10]. Though third- and fourth-generation biofuels show very promising and advantageous technology in the production of biofuel, the third-generation of biofuel has yet to be employed in massive applications since this concept requires a series of technical and biotechnology improvements [11]. Meanwhile, the fourth-generation of biofuel is still in an early stage and needs more research and time to develop into a feasible technology [12].

Generally, reactions involved in biofuel production require the use of a catalyst to facilitate the biofuel reactions, such as transesterification, esterification, hydrocracking, hydrodeoxygenation, and deoxygenation. Catalysts can be divided into three classes: homogeneous catalysts, heterogeneous catalysts, and enzymes. A homogeneous catalyst is a type of catalyst that is usually dissolved in a solvent and operates in the same phase as the reactants. Homogeneous catalysts are easier to operate than heterogeneous catalysts. However, homogeneous catalysts have challenges in separating products. A homogenous acid catalyst is suitable for being used for feedstock with high free fatty acid (FFA) content, but the downside is that it is highly acidic and has a slow reaction time [13]. Note that homogeneous catalysts also cannot be recovered after reaction, and therefore these homogeneous catalytic systems are difficult to commercialise. Due to this, the use of heterogeneous catalysts in biofuel production reaction is focused [14]. Heterogeneous catalysts are eco-friendly catalysts as they are easily recycled and separated from the biofuel product [15]. There are various types of heterogeneous catalysts, such as metal oxide, zeolite, sulfonic ionic exchanged resin, sulfonated carbon-based catalysts, and mesoporous catalysts [16]. Among these, metal oxide catalysts have been found to be advantageous, owing to their macroporous structures that are capable of speeding the organic transformations under solvent-free conditions and resulting in excellent catalytic activity. Pore volume, the presence of a large internal surface area, and porous metal oxides allow for a good control of reagent and product diffusion in the pores [17]. Although metal oxide catalysts have made a lot of progress in development and are widely tested in biofuel production, the reaction is still unselective [18]. The poor reaction activity is suggested due to the instability of the bulk character of active metal species. This bulk-character catalyst typically has low exposed active sites, as the active sites at the corner and edge, defects, and interfaces between the metal and support are missing. However, this problem could be overcome by atomically dispersing the active metal on the catalyst support [19].

In single-atom catalysts (SACs), supported SACs are made up of isolated individual atoms scattered on and/or coordinated with the surface atoms of appropriate supports (also known as hosts), which not only improves metal atomic efficiency but also provides an alternative method for regulating the activity and selectivity of catalytic processes. The strong host–metal interactions are responsible for the thermal stability of SACs, hence maintaining the single atom's isolation [20]. The historic evolution of scholarly works on SACs from 2000 to 2021 is shown in Figure 1. Here, the statistics indicate an increment from 97 scholarly works in 2000 to 1118 in 2021. An unexpected, inverted volcano curve of the trend of academic work on SACs was noticed. The year 2018 was the most active for SAC research.

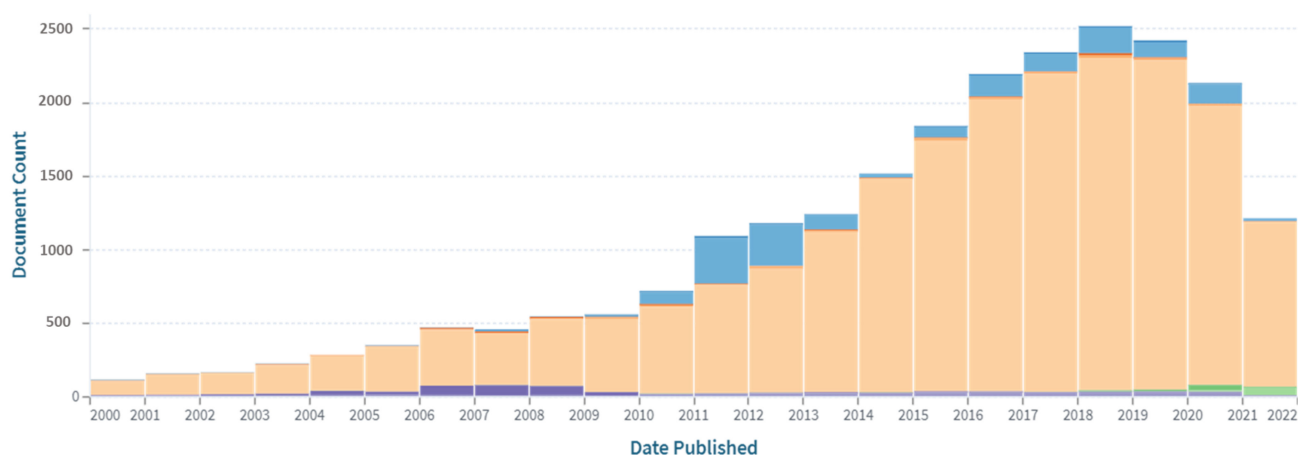


Figure 1. The annual number of scholarly works on SACs. (The Lens scholar analysis search system (formerly Patent Lens): search term “single-atom-catalyst” within 2000–2021. <https://link.lens.org/UXZ0NOGgH3i> (accessed on 11 October 2021)).

SACs are apparently used in the processes of transformation of gas or liquid towards the production of small molecules for fine-chemical development. It is worth noting that SACs are typically combined with a nanoparticle (NP) catalyst; SACs are positively charged owing to the absence of metal–metal bonds, which differs from the NP catalyst [21]. Based on the various SACs’ catalysed reaction processes, there are two areas that promise revolutionary breakthroughs for SACs: first, they are employed as an alternative substitution for precious-metal-based catalysts in energy-related processes, and second, they are used as molecular catalysts in organic synthesis. Indeed, iron, cobalt, and nickel single atoms have proven to be the most effective active metals in most energy-related processes [22].

Aside from SACs, single-atom alloys (SAAs) have piqued the interest of researchers. To be more explicit, SAAs are materials generated by bi- and multi-metallic complexes, where one of these metals is atomically distributed in such a material. Apparently, the use of expensive active metals in SACs can be solved by the utilisation of a variety of alloys [20]. It is worth mentioning that the strong metallic interaction between isolated single atoms and the metal nanostructure/support (host) intrinsically induces the catalytic characteristic of SAAs’ active sites; as a result, new atomic and electronic structures are formed [23]. Indeed, by atomically dispersing the isolated single atom or SAAs on the catalyst support, the maximum active sites with the largest surface free energy may be realised, with the surface free energy being substantially higher than the bulk character catalyst (Figure 2A). It should be noted that, in comparison to SACs, SAAs maximise the metal’s atomic efficiency while also providing more consistent and well-defined active sites [23]. Surprisingly, recent research has shown that the majority of SAA catalysts exhibit remarkable catalytic behaviour in a variety of chemical reactions (e.g., hydrogenation, hydrogenolysis, H₂ evolution) [24–26]. Based on former literature, the effectiveness of SAAs is attributed to relay catalysis, a synergistic effect between metal–metal active sites. The effectiveness of SAAs is evinced by the findings of Zhang et al. [27]. Indeed, a large H₂ evolution was observed when the Pt/Pd SAAs catalyst was employed in a hydrogen evolution reaction (HER) and oxygen reduction reaction (ORR). Based on this study, it can be seen that the prepared Pt/Pd SAAs (Figure 2B) outperformed a commercial Pt/C catalyst for both of the reactions. Apparently, the excellent dispersion of single-atom noble metals was monitored using sub angstrom-resolution, aberration-corrected scanning transmission electron microscopy (STEM). Meanwhile, the atomic resolution high-angle annular dark-field (HAADF) was used to identify the heavy atoms. Based on these analyses, the individual metal atoms can be observed. This is evinced by the aberration-corrected high-angle annular dark-field scanning transmission electron microscopy (AC HAADF-STEM) images from Huang et al. (Figure 2C,D). Indeed, all the yellow circles exhibited the presence of isolated Co single atoms, as supported by EDX mapping and XPS (Figure 2E,F) [28]. Based on the aforementioned SAC and SAA findings, with 100% of metal dispersion and maximum

active metal sites exposure, both of the catalysts will be expected to be very effective for catalysing various types of biofuel reactions such as hydrodeoxygenation, photocatalytic water splitting, water–gas shift (WGS), and dry methane reforming (DRM) for the production of liquid fuel and gas fuel. In fact, many reaction studies have utilised SACs and SAAs as catalysts [20,23,29]. However, the influence of SACs and SAAs on biofuel reactions is still lacking. Despite the fact that the number of SAC and SAA catalysed reactions for biofuel production is limited, in this review we will continue to summarise current trends in the usage of SACs and SAAs for biofuel production. This is critical in determining the potential of SACs and SAAs for biofuel manufacturing processes. It should be noted that various methodologies for the synthesis of SACs and SAAs will be thoroughly examined. Finally, we briefly explore the upcoming problems and prospects.

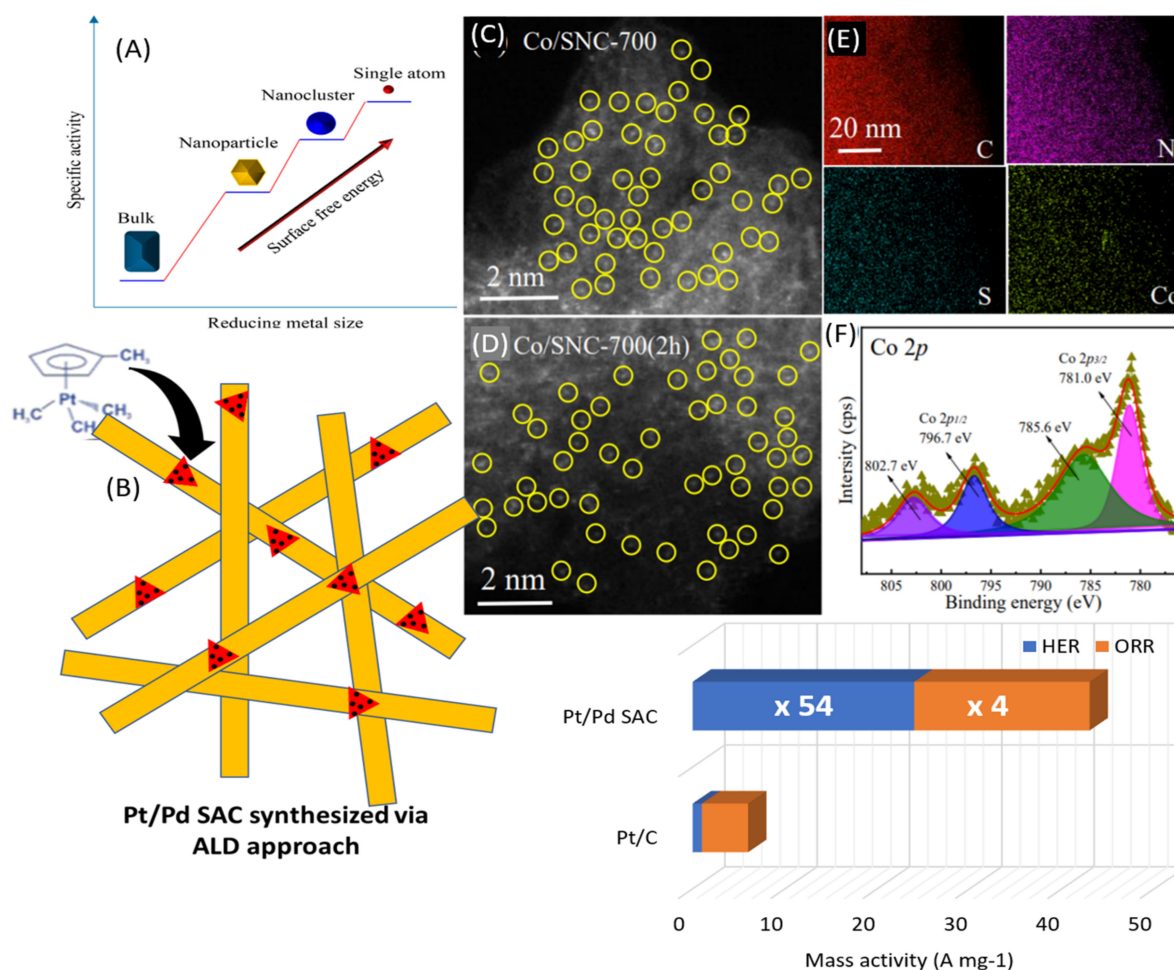


Figure 2. (A) The trend transformation of bulk-character NiCo surface free energy to SAC surface free energy. (B) Schematic proposed for Pt/Pd alloys structure for HER and ORR reactions. Adapted from [27], (C,D) the HAADF-STEM images for Co/SNC and Co/SNC after calcination at 2 h, (E) elemental composition of Co/SNC using EDX mapping, and (F) XPS pattern for Co/SNC. Adapted with permission from [28].

2. SAC and SAA Systems and Configuration

The reactivity and selectivity of heterogenous catalysts are affected by various factors (composition, shape, size of metal, surface area, pore size, acidity, basicity, metal dispersion, metal loading, etc.) [30–33]. Among these factors, the size of the metal constituent and metal dispersion have the greatest influence on the reaction activity, in which atomically dispersed metal is thought to have the maximal impact [30]. For that reason, significant attempts have been made to reduce the metal particles' sizes to an atomic level over the

years. Therefore, SACs and SAAs have garnered enormous attention for material synthesis and their potential applications towards various catalytic reactions [34,35]. Taking into consideration the ultimate low-coordination environment of single atoms, they are able to attain maximum metal dispersion for high exposure of each atom as a catalytically active site. On the other hand, the intrinsic quantum size effects of electron confinement are pivotal for discrete distributions of energy levels and distinguishing the highest occupied molecular orbital from the lowest occupied molecular orbital (HOMO–LUMO) gaps [36]. A decrease of the number of metal atoms in a particle will lead to narrower electronic bands, and in the end will be replaced by discrete states. Meanwhile, the density of d-states of single atoms will become broader as a result of single atoms' dispersion on the supports. The degree of the broadening mainly relies on the single atom–host interaction. Most importantly, the distinct electronic structures of SACs and SAAs are commonly attributable to their unique atomic-local environments that are believed to give an outstanding catalytic performance [37]. In regard to this, Ren et al. proposed a synthetic procedure to control the coordination environment of Pt single atoms on a Fe_2O_3 support [38]. This work demonstrates the existence of strong interactions between the coordination environment and the oxidation state of single atoms, which can be used to describe the model catalytic reactions.

SAAs' systems are often made of catalytically active metals that are atomically scattered in a less reactive metal host. Typically, SAAs are comprised of a noble metal matrix with metal atoms dispersed across the surface, so no bonds are formed between neighbouring active sites. The catalytic performance of SAAs mostly depends on their electronic properties. For example, the work done by Greiner et al. shows that the Cu d states of AgCu SAAs existed as free atom states, which gave rise to notably different catalytic activities from the monometallic Cu catalysts [39]. Owing to their unique bonding geometry, SAAs are potentially viable for changing the electronic structure of the solute atom [40]. Changes in electronic structure commonly involve a position shift in the d-band relative to the Fermi level.

3. Stabilized SAC and SAA Strategies

3.1. Stabilization of SACs

The stability of SACs has become one of the greatest challenges and it is extremely important that this impedes their broad applications in both fundamental and industrial applications. SACs are known to be thermodynamically unstable because of their high surface-free energy and low coordination number of free single atoms, which always sinter or ripen with time, causing them to change to the favoured thermodynamically state of fewer and larger particles [41,42]. Generally, there are two major factors that cause degradation of the stability of SACs: leaching and aggregation. However, the SACs can be stabilised by improving their mutual metal–support interaction and coordination geometric effect.

3.1.1. Mutual Metal–Support Interaction

The theory of mutual-metal support interaction was introduced by Tauster and his co-workers in 1978 when they first found the principle of mutual support interaction [43]. This interaction can be classified into two types: electronic defects and surface structural defects. Surface structural defects include a variety of surface defects such as surface vacancy, unsaturated site coordination, and surface step. All of these defects are used to trap a single metal atom to stabilise it. On the other hand, electronic defects are all about the interaction between single atoms and their hosts (supports), which is commonly related to reducible oxide supports such as TiO_2 , CeO_2 , and so on. Electronic defects manage to closely anchor individual atoms by forming $\text{M}_2\text{–O–M}_1$ formations or $\text{M}_2\text{–M}_1$ bonding, where M_1 is a single atom while M_2 is the host. Due to the supreme anchoring sites for single atoms with the advantages of multiple bonding, certain vacancies on particular supports will be obtained in this arrangement. Both types of interaction show a significant influence on the catalytic activity, selectivity, and stability of SACs [43–45].

According to some studies, modulating the interaction between a single atom metal and support can be well controlled by regulating the size of metal particles into nanoparticle-sized metal for catalytic processes [46,47]; as single atoms are thermodynamically unstable, they tend to form metal nanoparticles (NPs) or cluster in post-synthesis treatments at high temperatures (see Figure 3) [36]. Notably, anchoring single atoms on a support with a stronger metal–support interaction is one of the strategies for SAC stabilisation [48–50]. These interactions cause charge transfer and mass transport (via migration movement) from supports to a single metal atom [51], that would not just lead to the stability of the atoms, but would also have a significant effect on their electronic structures, hence boosting the catalytic performance [52,53]. Few studies have been done in order to define the stability of SACs in terms of binding energy (E_{bind}) of a single metal atom to the support [54,55].

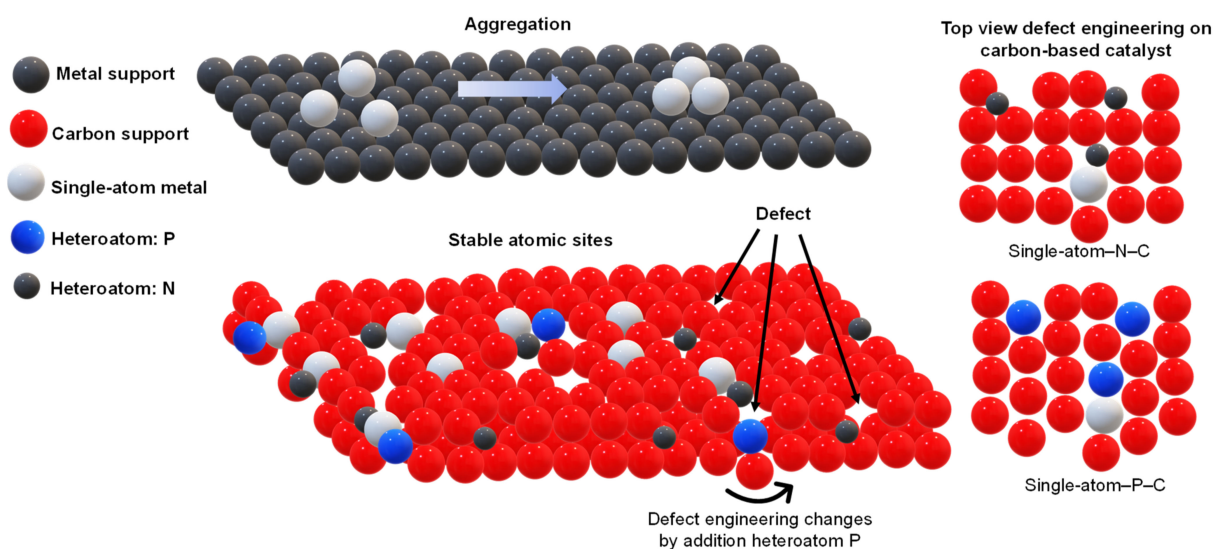


Figure 3. Illustration of heteroatoms-doped metal and carbon support.

There are two early approaches in immobilising and enhancing SAC stability: (i) capturing organometallics into the micropores of the support and (ii) anchoring organometallic catalysts through organic linkers or weak interactions. However, there is no direct interaction between the metal centre and the supports in both approaches [30]. Hence, to confine single atoms, they can be physically trapped in micropores or chemically grafted onto the frameworks of microporous matrices such as metal organic frameworks (MOFs). According to the latter method, surface species on the supports behave like ligands that trap single atoms for metal atoms' isolation and stabilisation.

Even though great efforts have been devoted to this, the low-porosity structures and ultra-low metal loading (generally < 1.0 wt.%) of these catalysts are still a major challenge. Moreover, the metal atoms are prone to forming a large degree of aggregation due to a lack of anchoring groups of supports for metal stabilisation or the relatively weak interactions between the metals and hosts [56]. Due to this matter, recent studies show that the most suitable substrate to anchor is carbon because it has a highly specific surface area, excellent electrical and thermal conductivity, and is highly stable under harsh conditions [57]. Moreover, carbon-based supports have a flexible surface, so they can be adjusted accurately with engineering defects. Hence, due to these special properties, heteroatom dopants or external ligands are introduced to carbon-based catalysts so that more anchoring sites to stabilise single metal atoms are offered. For example, nitrogen and sulphur dopants as lone-pair electrons tend to trap single metal atoms and form strong chemical bonds [58,59]. As demonstrated by Figure 3, different heteroatom dopants create different kind of defects. In contrast to the widely studied N-doped support, the presence of P atoms as dopants into the carbon framework favours the formation of a distorted configuration attributable to its larger size and lower electronegativity as compared to N

atoms [60]. Moreover, the P species are easily oxidised to PO_x with electron deficiency and slow down the formation of defects, which is essential for anchoring single metal atoms.

Alternatively, the anchoring of metal atoms can also be attained by the defective sites of the catalyst support matrix as a substitutional or interstitial dopant and also by forming metal-vacancy complexes with much higher binding energies [29]. In the past few years, countless anchor species have been used in synthesizing for isolating the metal species on the host matrix. The anchor species, also known as coordination atoms, that have been studied include B, C, N, O, S, and P [61], where each metal atom coordinates with three and four coordination atoms. According to the stability screening test, C and N are further verified as the best coordination atoms which mostly acquire both threefold (3C) and fourfold (4N) configurations. The descriptor was then used to analyse the catalytic activity of the designated combinations based on the free energy of hydrogen adsorption on the metal centres. The results from screening showed that most of the active and stable catalysts were correlated to the 3C configuration as a result of the free orbitals of the threefold-coordinated metal centre which strongly interact with the hydrogen 1s orbital.

Work by Bulushev et al. has shown homogeneously dispersed and well stabilised single-atom Ni supported on N-doped carbon (1Ni/CN) and its parent carbon (1Ni/C). Highly stabilised and isolated single-atom Ni has been proven by HAADF-STEM findings (Figure 4A,B). Notably, both catalysts exhibited a superior transformation of formic acid into hydrogen (Figure 4C) [62], in which the reaction is predominated by 1Ni/CN as a result from the strong Ni atoms–N-species interaction on the carbon support (See XPS result, Figure 4D). Cheng et al. also successfully synthesised a single cobalt atom anchored to N-doped carbon nanofibers (CNFs) [63]. Overall, the synthesised catalysts possess strong metal interaction with solid support as evidenced by aberration-corrected STEM (Figure 4E,F) and HAADF-STEM (Figure 4G,H) images. The catalysts show a promising performance, in which no loss of catalytic activity in electrochemical reactions is observed (Figure 4I).

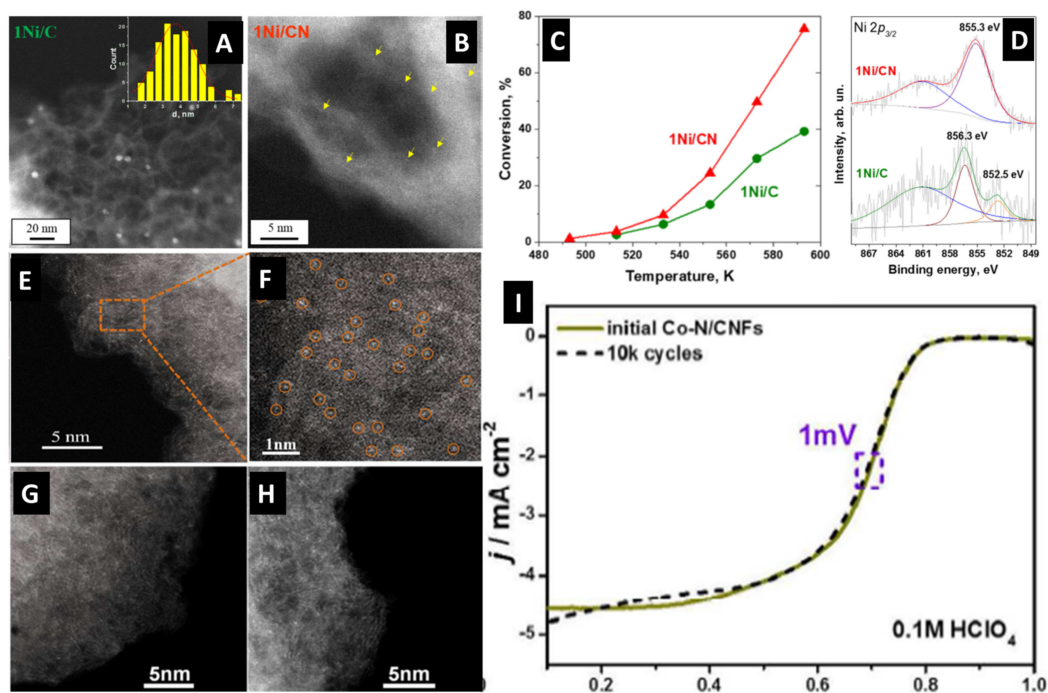


Figure 4. (A,B) HAADF-STEM images for 1Ni/C and 1Ni/CN (yellow arrow shows isolated single-atom Ni), (C) formic acid conversion into hydrogen, and (D) Ni $2p_{3/2}$ XPS deconvolution peaks for 1Ni/C and 1Ni/CN. Adapted with permission from [62], (E) aberration-corrected STEM image, (F) enlarged images of Co-N/CNFs (orange circle: single-atom Co), (G,H) HAADF-STEM images of Co single atoms in different regions for Co-N/CNFs catalyst, and (I) stability test of Co-N/CNFs within 10,000 cycles in O_2 -saturated 0.1 M HClO_4 . Adapted with permission from [63].

Undeniably, improving the interaction between a metal atom and a host is believed to be the right answer for stabilising the SACs on a catalyst support or host matrix [64], and this can also be achieved by functionalizing with suitable “anchor” groups such as carboxyl, hydroxyl, and amide groups [65,66].

Nonetheless, interatomic interaction has a varied effect on atomic number and the configuration of the coordination environment because the electronic structure of active metal sites shows a noticeable catalytic activity and selectivity.

3.1.2. Coordination Geometric Effects

Special locations of single atoms and strong metal–strong interaction (SMSI) causes the supported SACs to have unique geometric and electronic properties. Another example of the geometric effect of SACs is the homogenised active sites, which are all well-defined and atomically dispersed on the supports. This results in an identical geometric structure of each active centre, and is comparable to a homogeneous catalyst [67]. The SACs’ geometrical pattern can be varied by two factors: the coordinates (coordinate number) and the types of coordinates bonded to the metal centres (type of bonding). For SAC stabilisation, it has been demonstrated that the coordination geometric effects play a crucial role in enhancing interactions between metal atoms and coordinatively unsaturated sites (Figure 5A) [68]. For instance, the work of Tang et al. demonstrates the anchoring of single-atom Ru catalysts on alumina supports that contain a high content of coordinatively unsaturated Al^{3+} sites [69], which contributes to the presence of abundant defects on the support that are able to trap single atoms. The formation of strong interactions between Ru and Al^{3+} species was determined to modify the electronic and geometric properties of metal atoms, which led to an excellent catalytic activity for the hydrogenation reaction of benzene.

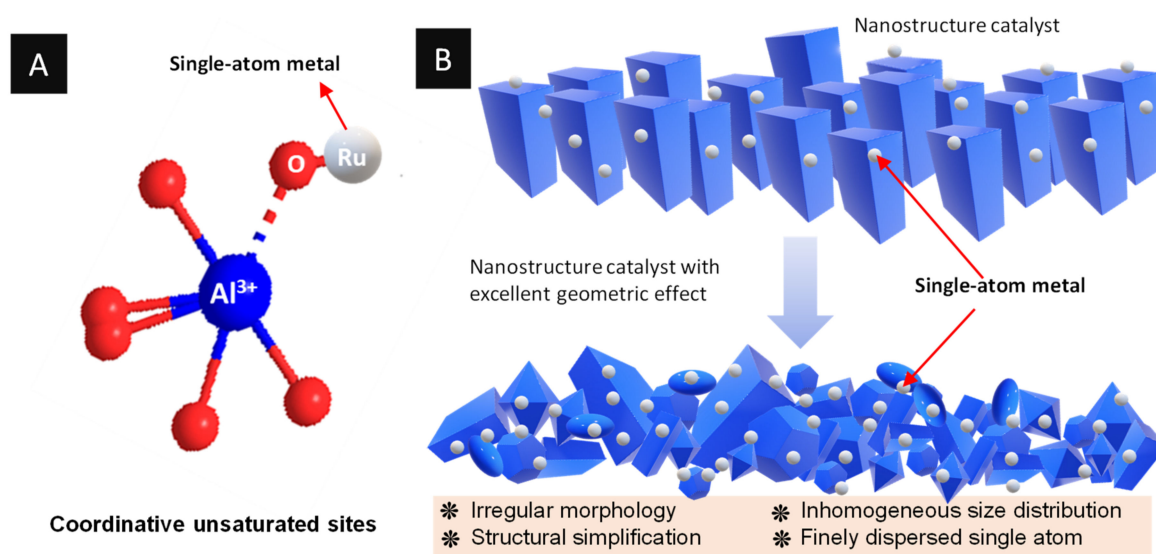


Figure 5. Illustrations of (A) SACs on unsaturated sites of Al^{3+} support and (B) geometric effect on nanostructure catalyst.

As illustrated in Figure 5B, the geometric effect can enhance the stability of SACs by reducing the size of the nanostructure catalyst for the dispersion of single atoms. According to previous research [70,71], the irregular morphology and inhomogeneous size distribution are responsible for the wide range of reaction active centres. Later, structural simplification is also beneficial for SACs. The benefit of finely dispersed isolated active centres over the supports and well-designed isolated active centres is their high selectivity due to the similarities in the coordination environment in each reaction centre [72].

The effect of coordination geometry on the stabilisation of SACs is shown in a few studies. Wei and co-workers studied the function of contiguously located Pd sites and found that the rate of the determining step changed with the formation of Pd single atoms

on the Au surface [73]. Next, Song and co-workers found that differences in chemical potential caused by charge transfer between single atoms and the support result in anchored single atoms carrying charge [74]. Later, Jiu Liu and co-workers found that the bonding or coupling of quantum levels of single metal atoms with surface species is caused by the conjunction of a single metal atom with the surface groups of supports. For example, an experiment on Pt₁/FeO_x SAC conducted by Qiao and co-workers showed that, when anchored on FeO_x, Pt atoms are positively charged and the discrete 5d-orbitals of Pt atoms are evolved to d-bands as they mix considerably with the O_{2p} band [67]. Thus, it can be concluded that the electronic properties of the catalyst will be altered by upgrading the coordination of single atoms with a support while metal–interaction that can overcome the catalytic process that requires multi-atom sites decreases [67,72].

3.2. Stabilisation of SAAs

While SACs are stabilised by metal–support interaction and coordination geometric effects, the stability of SAAs can be achieved by being alloyed with another metal via chemical bonding [21]. When it comes to SAAs, there are two major parameters that need to be considered for their stability: aggregation energy (a thermodynamic parameter determined by the relative stability of individual dopant atoms to dopant clusters) and segregation energy (a relative stability of the dopant inside the host versus bulk) [20,75]. Since SAAs exhibit superior surface free energy, the segregation energy is negative, implying that the dopant is highly stable in bulk character [76]. Moreover, aggregation energy is another parameter that is crucial for obtaining stable SAAs. In order to form an SAA, two metals need to possess a positive aggregation energy because those with negative values can cause the formation of clusters by the dopant atom. Zhang and colleagues, for example, investigated the segregation and mixing energies of various dopants such as Cu, Ni, Ag, Sc, Ti, V, Cr, Mn, Fe, and Co in the Ag(111) system. Notably, dopants were detected in the subsurface without adsorbates, with only Sc and Zn exhibiting mixing enthalpies (H) with negative values, in which site isolation tends to occur in the surface layer [77]. In another study by Fu and Luo, they discovered an absence of thermodynamic (H) inclination in the case of noble metals (Ru and Os) and transition metals' (Fe and Co) dopant site isolation on a Cu metal host, with an exothermic condition (release energy as heat) caused by the rearrangement of isolated sites into trimers [78]. Nevertheless, the dopants in the surface layer are not segregated to the bulk, which might be assisted by relatively weakly bound adsorbates. A specific alloy structure using ethene and acetylene and CO as adsorbates has been demonstrated to have the ability to induce an excellent aggregation of particles and homogeneously disperse the atoms into isolated forms as a function of adsorbate surface coverage in theory under vacuum [79]. Meanwhile, strong binding adsorbates such as acetylene promote agglomeration [80], but weaker binding adsorbates such as Pt and Pd do not [75,79]. In addition, at the initial state of alloying, the kinetic studies using a model system of alloy formation can also become a useful guide for stable SAAs. A dopant atom would be able to be placed at every site on the surface by controlling the alloying temperature, followed by a density functional theory (DFT) simulation test of each site.

4. SAC and SAA Support

According to the preceding explanation, catalytic support is advantageous for the stabilisation of SACs since different supports can serve as distinct anchoring sites for single atom stabilisation attributable to the varied chemical bonding of metal atoms and supports [71]. To date, oxide-supported SACs are one of the most largely explored systems among the various kinds of supported SACs [81,82], owing to their definite and variable properties such as acidity or basicity of the surface, as well as redox behaviours that can contribute to specific catalytic properties [82–84].

Kwon et al. reported on the dispersion of rhodium SACs on a zirconia support for the selective activation of methane by the wet impregnation method [52]. Due to the stabilisation of single-atom Rh on a zirconia support, it is not only able to activate methane

in mild conditions but is also able to convert methane to methanol using H_2O_2 in the form of an aqueous solution under a closed cycle of catalytic activity. Moreover, the conversion of methane to ethane using O_2 under gas phase below $300\text{ }^\circ\text{C}$ could be achieved as well. DRIFTS measurement and DFT calculation were implemented to ensure the stabilisation of CH_3 intermediates on the single-atomic Rh_1/ZrO_2 upon methane adsorption. Meanwhile, Xu and co-workers prepared a stable Pd single atom on the high-entropy fluorite oxide $(\text{CeZrHfTiLa})\text{O}_x$ (HEFO) support, Pd_1 @HEFO SAC, by simple mechanical milling followed by a calcination process [85]. From the HRTEM image, no agglomeration or sintering of the Pd species was detected, suggesting the possible existence of isolated Pd sites. Furthermore, the atomic dispersion of Pd on the HEFO was confirmed by HAADF-STEM and extended X-ray absorption fine structure (EXAFS) results. The incorporation of single Pd atoms into the HEFO sublattice produces stable Pd–O–M bonds ($\text{M} = \text{Ce}/\text{Zr}/\text{La}$), contributing to the enhanced reducibility of lattice oxygen, hence demonstrating a higher low-temperature CO oxidation activity with excellent resistance to thermal and hydrothermal degradation. Another example of oxide supported SACs was reported for the preparation of Ir single atoms supported on FeO_x (Ir_1/FeO_x) via the coprecipitation method [86]. Even though the loading of Ir is extremely low, Ir_1/FeO_x SAC possesses significantly high activity for the water–gas shift reaction. The reaction rate of the present catalyst is 1 order of magnitude higher than its clusters and nanoparticle counterparts. Based on thorough analyses, single atoms are responsible for 70% of the total activity, suggesting that the important active sites originate from Ir atoms. Fu et al. reported on the synergistic effect of dual SACs supported on TiO_2 ($\text{Ir}_1\text{Mo}_1/\text{TiO}_2$) which was responsible for a better catalytic chemoselectivity with 96% at 100% conversion compared to an Ir_1/TiO_2 SAC [87].

Owing to its high vacancy density, ceria (CeO_2) has become one of the promising supports that can stabilise single metal atoms [82]. Han et al. created a single Rh atom supported on CeO_2 for a low-temperature CO oxidation reaction [88]. An excellent activity of CO oxidation as well as good stability were attained on active sites of the single atom through the Mars–van Krevelen mechanism that can also prevent low temperature CO poisoning. The proposed mechanism has been confirmed by CO-DRIFTS and kinetic studies. Other work on CeO_2 -based support materials was done by Zhou and co-workers [89]. They investigated a high-loading Pt SAC on a CeO_2 -modified diatomite support for the hydrogenation of phenylacetylene to styrene. Modification of diatomite with CeO_2 nanoparticles increased the defect sites of the support, which is important for a high loading of single atoms. The good performance of the selective hydrogenation was achieved due to an improved metal–support interaction.

MoS_2 materials have been extensively studied, especially in the application of electrocatalytic HER due to their unique structure and electronic properties as a result from the coordination of unsaturated sulphur (S) atoms along its edges [90]. Zhang et al. synthesised single-atom Ru supported on a MoS_2 (SA-Ru- MoS_2) electrocatalyst for HER [91]. They found that single-atom Ru as a dopant causes a MoS_2 phase transition and S vacancies, which remarkably enhances the HER performance of MoS_2 . The synergy effects between single-atom Ru doping and S vacancies mainly contribute towards significantly high HER activity, as demonstrated by DFT calculations. A comparable study was done by Wang et al., in which single-atom Ni was decorated on a MoS_2 support for the same purpose as HER [92]. Atomic STEM data show the anchoring of Ni single atoms on the S-edge and H sites of the basal plane that are responsible for the enhancement of HER activity.

In the case of SAAs, a small amount of an isolated single metal atom is present on the surface layer of the metal host [20]. For example, Liu et al. synthesised a PdAu SAA catalyst for the selective hydrogenation of 1-hexyne in the liquid phase [93]. The as-prepared PdAu SAAs and SAAs supported on silica were both prepared to investigate their activity. They demonstrated that the PdAu SAA catalyst shows an outstanding selectivity and stability for the hydrogenation of 1-hexyne to 1-hexene. This is mainly attributable to the enhancement of hydrogen activation on PdAu SAA. It is worth noting that the catalytic performance of supported PdAu SAA on silica is similar. Therefore, silica support is not necessarily

required for catalytic performance. The summarisation of the various types of supports and metal hosts used as supports in SAC and SAA catalysts are shown in Table 1.

Table 1. Summarisation of supported SACs and SAAs.

Catalyst	Preparation	Performance	Ref.
Rh/zirconia SAC	i. Preparation of zirconia support by sol-gel method ii. Deposition of Rh on zirconia by a wet impregnation method	Activation of methane in mild conditions by single atomic Rh catalysts on zirconia support.	[52]
Pd/fluorite oxide (CeZrHfTiLa) _x (HEFO)SAC	Combination of mechanical milling with calcination at 900 °C	Incorporation of single Pd atom into HEFO by forming stable Pd–O–M bonds (M=Ce/Zr/La). The reducibility of lattice oxygen has been improved with higher CO oxidation activity at low-temperature and superior resistance to thermal and hydrothermal degradation.	[85]
Ir/FeO _x (Ir ₁ /FeO _x) SAC	Co-precipitation method Aqueous mixture of H ₂ IrCl ₆ and Fe(NO ₃) ₃ with appropriate ratio was added dropwise to NaOH solution (pH of the final solution was maintained at around 8)	The activity is 1 order of magnitude higher than its Ir cluster or nanoparticle counterparts and even higher than those of the most active Au- or Pt-based catalysts.	[86]
Ir ₁ Mo ₁ /TiO ₂ SACs	i. TiO ₂ support was treated at 600 °C for 2 h under argon ii. Ir ₂ Mo ₂ (CO) ₁₀ (η ⁵ -C ₅ H ₅) ₂ was dissolved in dry n-pentane, forming an orange colour solution iii. TiO ₂ support was added to the previous orange solution, followed by vigorous stirring overnight until the orange colour was not observed iv. The solvent was removed by evacuation using Schlenk techniques, then was heated at 450 °C under argon	Dual single-atom catalyst supported on TiO ₂ , Ir ₁ Mo ₁ /TiO ₂ SACs demonstrate a superior catalytic performance for selective hydrogenation of 4-nitrostyrene (4-NS) to 4-vinylaniline (4-VA) as compared to single-atom catalyst Ir ₁ /TiO ₂ .	[87]
Pt/CeO ₂ modified diatomite SAC	Dispersion of diatomite in the solution of 1,3,5-benzenetricarboxylic acid and Ce(NO ₃) ₃ mixture, followed by calcination. CeO ₂ @diatomite was dispersed in solution of H ₂ PtCl ₆ and further calcined in air at 300 °C	Highly active for hydrogenation of phenylacetylene to styrene	[89]
Rh ₁ /CeO ₂ SAC	Co-precipitation method	Highly active and good stability for CO oxidation (TOF of 0.41 s ⁻¹ at 100 °C).	[88]
Ru/MoS ₂ SAC	Simple one-step impregnation method RuCl ₃ was added into a MoS ₂ nanosheet dispersed in a mixed solution of ethanol and deionised water	Significantly improved hydrogen evolution reaction (HER) of 2D MoS ₂ (low overpotential of 76 mV at 10 mA cm ⁻² in alkaline media).	[91]
Ni/MoS ₂ SAC	MoS ₂ on carbon cloth was immersed into NiCl ₂ ethanol solution before being dried at 80 °C, followed by calcination at 300 °C for 1 h under 10% H ₂ /Ar atm	Enhanced HER activity (98 mV and 110 mV in 1M KOH and 0.5M H ₂ SO ₄ , respectively).	[92]
PdAu SAA PdAu/silica SAA	Sequential reduction method (Pd/Au ratio of 1/250) Fumed silica was introduced into PdAu SAA solution in water and stirred overnight	Excellent selectivity and stable activity of PdAu SAA for the hydrogenation of 1-hexyne to 1-hexene. Silica support is not required to catalyse the reaction.	[93]

Obviously, most single atoms interact with support materials for high dispersion in order to avoid the formation of clusters. Strong single atoms–host/support interaction has been proven to promote the excellent performance of catalytic activity in various applications. Based on the aforementioned findings in Table 1, SAC and SAA supported catalysts still suffer from a low-porosity structure, which would increase the resistance to mass transport, leading to poor catalytic activity. Therefore, the utilisation of porous and large-surface area hosts or catalyst support is necessary as it can provide many more available sites for the attachment of metal atoms [94,95]. Moreover, the aggregation of metal atoms can be avoided by the pore structure of porous materials, which enhances the metal atom loading.

Graphene (GN) is an advanced carbon nano-material with a two-dimensional single sheet of carbon atoms arranged in a hexagonal network. GN is a material that has a large specific surface area (high catalyst loading) and good stability (tolerance to harsh operational conditions [96]). Under realistic catalytic conditions, GN also has extraordinary physicochemical properties such as a high mechanical strength and thermal stability [48]. An ideal GN structure (large surface area) can be achieved by using the mechanical exfoliation technique. Using this method, the surface area of GN can be obtained up to 2630 m²g⁻¹, which is an ideal structural system for improving the distribution of metal atoms. Undeniably, this will maximise the exposure of the catalytic centres to the reac-

tants [97]. It should be noted that modifying the GN sheets will also result in a porous structure and, apparently, it will increase the accessible surface area. Indeed, untreated GN sheets are inappropriate to be used as SACs and SAAs because the dangling-bond free GN sheets consist of highly mobile adatoms and could easily aggregate as a result of their low migration energy barrier. It should be noted that the presence of an adatom on GN will prevent the bonding configuration for the metal atoms. For this reason, the formation of defective sites in GN is necessary as the defective sites will provide numerous possible bonding configurations for metal atoms, thus stabilising the SACs and SAAs. One of the common methods that has been widely used in the powder production industry is ball milling, which applies kinetic energy to the materials through the movement of balls. This method reconstructs the chemical bonds of materials and produces fresh surfaces [98]. For GN production by the exfoliation of graphite, the ball milling method has also been implemented. This also involves the fragmentation and chemical functionalisation of GN [99]. Very recently, work by Deng et al. showed the preparation of well-dispersed single atoms (FeN_4) confined in the GN matrix by applying a ball milling strategy to iron phthalocyanine (FePc) and GN sheets. Interestingly, the FeN_4/GN was successfully prepared in a large quantity [48]. Based on the images obtained from HAADF-STEM and LS-STM analysis in this study, the FeN_4 centre was obviously embedded in the graphene lattice. This approach was then implemented by the same group to prepare various atomic 3d transition metals such as Mn, Fe, Co, Ni, and Cu within graphene lattices [29,100].

As a result of N-doping into the carbon network, the electronic properties of carbon will be modified, making carbon nitride (CN) a promising porous support material for single atoms. Compared to C, it is much easier for metal atoms of SACs to coordinate with N due to the presence of the lone electron pairs of N. This will lead to the coordination of most metal atoms of SACs with N to form M-N_x (M: metal atom) [101]. There has recently been a report on SAC preparation by confining single Fe atoms in CN [102–104]. All of these Fe SACs demonstrate a superior catalytic performance with excellent stability. In order to fulfil industrial needs, it is undoubtedly essential to synthesise SACs within CN on a large scale. This work has been realised by Zhao et al. in the development of a large scale metal-NC SAC series [105]. Indeed, an optimum metal loading was found to be 12.1 wt.% for the maximum electrochemical CO_2 reduction reaction (CO_2RR).

Zeolite is another important porous material that has been widely used in various applications such as thermocatalysis and dehydrogenation/hydrogenation [106]. Taking into account the uniform pore and cage structure of zeolite, the metals can be uniformly distributed in these structures, and are thus strongly confined to the metal atoms. Liu et al. prepared single-atom catalysts confined to zeolites through an in situ synthesis method in the zeolite crystallisation process. The metal and ethylenediamine were complex, forming a precursor to avoid the precipitation and aggregation of metal [107]. The aberration-corrected high-angle annular dark-field scanning transmission electron microscopy (AC-HAADF-STEM) analysis showed the presence of single metal atoms, which are represented by bright dots that are clearly different from the zeolite. In contrast to the impregnation method, the precursors are commonly assembled in the shallow layer of the zeolite crystals because of the limitation of micropore diffusion. It can be observed that the uniform dispersion of the precursors in the entire block was successfully implemented by this in situ synthesis strategy. Moreover, the most stable configuration demonstrated by DFT calculation and EXAFS consists of metal atoms that were coordinated with two oxygen atoms in Al–O–Si bridges and the six rings of the zeolite Y framework for Pt atoms. On the other hand, Sun and co-workers applied one-pot hydrothermal synthesis conditions followed by H_2 reduction for rhodium atoms encapsulation within MFI silicalite (S-I) and ZSM-5 zeolites [108]. Based on the EXAFS analyses, due to the formation of superfine Rh species, all zeolite-encaged Rh species had a higher oxidation state than the Rh foil, resulting in a high efficacy in the tandem hydrogenation of nitroarenes by coupling with ammonia borane (AB) hydrolysis.

Metal organic frameworks (MOFs) are one of the promising well-dispersed metal catalyst porous support materials owing to their ability to provide coordination sites for metal atoms by introducing metal species into tunable inorganic metal nodes and organic ligands [109]. Li et al. used a single-ion capture method to develop a stable single-atom catalyst in an MOF-808 structure [110]. This approach involved an exchange of an ethylenediaminetetraacetic acid (EDTA) ligand with the original ligand that anchored on the metal node of the Zr_6 cluster. This has been proven to effectively capture a single metal ion with excellent photocatalytic hydrogen evolution activity and also high stability. DFT data revealed that the outstanding performance was correlated to the lower free energy of hydrogen binding that has been efficiently produced by Pt atoms under photocatalytic conditions. Apart from single atom incorporation into the MOF, the formation of defects in MOFs is very useful for anchoring metal atoms. For example, the work done by Guo and co-workers demonstrated the anchoring of Pt atoms in a Ce-MOF caused by the formation of defects [111]. This provided an abundant active site for CO conversion resulting from the strong interaction between isolated Pt atoms and ceria in the MOF. Zhao et al. also reported that the formation of defects in an MOF assists in anchoring metal atoms in order to obtain a high-quality SACs [112].

5. Synthesis of SACs and SAAs

Bottom-up synthesis strategies and top-down synthesis strategies are the two types of SAC and SAA synthesis strategies.

5.1. Bottom-Up Synthesis Strategies of SACs and SAAs

Bottom-up strategies such as atomic layer deposition (ALD), co-precipitation and wetness impregnation are traditional methods for the development of SACs. The ALD technique is a practical technique to use to synthesise single metal atoms on graphene or other supports. ALD is beneficial for synthesising desired SACs because it has precise control over the growth of metals that will construct composites with a variety of morphological features. Unfortunately, the ALD process yields a lower amount of SACs, making it less appealing to industry [1,3]. Interestingly, the SACs produced by the ALD method have greater stability properties. This is evinced by Nongbe and co-workers in the development of sulfonated graphene ($GR-SO_3H$), whereby insignificant metal leaching was observed after being used in biodiesel synthesis [113]. Sun et al. discovered a similar trend over Pt/graphene for methanol oxidation, demonstrating strong catalytic activity at 0.59, 0.60, 0.62, and 0.70 V and stability with 50, 100, and 150 ALD cycles [114].

Co-precipitation is the most popular approach for producing SACs, in which chemicals that would normally dissolve under the conditions are expedited. This method has several advantages, including a simple synthesis stage, low cost, and it saves more time. This was evinced by Qiao et al. in their development of nanocrystalline Pt_1/FeO_x SAC, utilizing $H_2PtCl_6 \cdot H_2O$ as a metal antecedent blended in with $(Fe(NO_3)_3 \cdot 9H_2O)$ in a legitimate molar proportion and pH [35]. The results revealed that single Pt atoms were homogeneously distributed on the FeO_x SAC surface with a metal loading level of 0.17 wt.%, resulting in an extraordinarily high atom productivity. The Pt_1/FeO_x SAC catalyst exhibited a greater strength and prevalent movement for both CO oxidation and the special oxidation of CO in H_2 . Similar trends were observed by the research group of Qiao [115], whose results showed that Au_1/CeO_2 SAC and Au_1/FeO_x SAC, which were prepared via the co-precipitation method, exhibited a higher CO conversion (60–90%). It can be noted that the co-precipitation method has also been used for synthesizing Pt_1/ZnO SAC and Au_1/ZnO SAC [116]; both Pt_1/ZnO SAC and Au_1/ZnO SAC exhibited high methane conversion rates (28–43%) and a high CO_2 selectivity (88–100%) during methanol steam reforming processes. This synthesis method was also found to be effective in the development of a Ru/CoFe-LDH SAC for electrochemical reactions using CoFe-LDHs and $RuCl_3 \cdot H_2O$ as a metal precursor. According to their findings, the RuCoFe-LDH SAC catalyst only requires 198 mV of overpotential in basic solution to produce a current density of 10 mA

cm², making it one of the best OER electrode materials. Furthermore, XAS measurements revealed high synergetic electron interactions between individual Ru metal atoms and LDH substances, which can increase OER activity and stability when compared to CoFe-LDHs or commercial RuO₂ catalysts [117].

Galvanic replacement (GR), incipient wetness co-impregnation, physical vapour deposition (PVD), and ALD techniques are the basic methods for the preparation of SAAs. Galvanic replacement (GR) is a straightforward response driven by the distinction in electrochemical potential between two metals in an arrangement and is a broadly utilised strategy for making hollow nanostructures for use in catalysis, plasmonic, and biomedical examination [118]. The Pd_{0.18}Cu SAA was successfully synthesised by Boucher and co-workers using GR [119]. Cu NPs were made by mixing Cu(NO₃)₂ with poly(vinylpyrrolidone) PVP (MW: 40,000–80,000) at a molar ratio of Cu: PVP (1:1 wt./wt.), which then underwent a chemical reduction process using NaBH₄ under a N₂ atmosphere. Following that, Cu/Al₂O₃ was supported on alumina at 250 °C in a H₂ atmosphere, and the necessary amount of Pd (NO₃)₂ was introduced to the suspension with sonicating tips immersed in the suspension to increase the GR reaction. The results of UV-Vis spectroscopy and XPS examination showed that Pd was spread uniformly on the Cu nanoparticles. Furthermore, Shan and colleagues produced Pd₁Cu SAA, Pt₁Cu SAA, and NiCu SAA via GR for ethanol dehydrogenation, and the results revealed that the NiCu SAA has a higher activity in ethanol dehydrogenation than Pd₁Cu SAA and Pt₁Cu SAA. This is due to the presence of Ni, which decreases the C–H activation barrier and thus increases the activity [120]. Similarly, Marcinkowski and colleagues [121] studied Pt/Cu SAAs for C–H activation, whereas Lucci and co-workers produced the same catalyst for the hydrogenation reaction via the GR method as in the schematic diagram shown in Figure 6A [122]. The HAADF-STEM (Figure 6B) result showed that Cu metal particles with reduced Pt atoms exhibited a grid dispersion of Cu of 0.21 nm at a 2 nm scale. Moreover, EXAFS (Figure 6C) analysis revealed the formation of a Pt–Pt bond in Pt/Cu alloys, indicating that Pt_{0.1}Cu₁₄/Al₂O₃ and Pt_{0.2}Cu₁₂/Al₂O₃ have isolated Pt atoms whereas Pt₂Cu₆/Al₂O₃ formed a Pt cluster. The GR method has also been used in transforming CuMgAl-LDH (layered double hydroxide) to PtCu SAA by partially substituting the Cu species with Pt ions by the GR method [24]. PtCu SAA catalysts with various Pt/Cu atomic ratios (atomic ratio: 0.010 to 0.015, 0.030, 0.15, and 0.50) were also investigated. However, when using the GR method, the support must be larger than the active metal to avoid metal host shrinkage if the contrary situation occurs [123].

Incipient wetness co-impregnation followed by physical vapour deposition (PVD) procedures are currently the most extensively utilised SAA catalyst synthesis methods. Gong et al. used an incipient wetness co-impregnation approach on a γ -Al₂O₃ support to make a thermally steady PtCu-(γ -Al₂O₃) SAA catalyst for the synergist dehydrogenation of propane. The results demonstrated that the propylene selectivity in the dehydrogenation activity over the Pt_{0.1}Cu₁₀ SAA catalyst was significantly improved [124]. The incipient wetness co-impregnation approach has also been used by Aich et al. in the development of Pd–Ag/SiO–SeqIWI SAA catalysts and monometallic pure Ag/SiO₂ catalysts for hydrogenation reactions. Pd–Ag/SiO–SeqIWI was found to be more catalytically effective than Ag/SiO₂ [125]. The same catalyst synthesis approach has also been applied by Kim et al. in the development of the Pt₁/ATO (antimony doped tin–oxide) support SAA catalyst in electrochemical reactions for H₂ production. Interestingly, the existence of individual Pt atomic sites positively influences reaction activity. Indeed, the Pt₁/ATO SAA catalyst shows an outstanding longevity [126].

PVD is a process that includes transporting elements at the atomic scale in a vacuum condition, utilising electron beam evaporators to produce the vapour deposition of confined metal particles onto a subsequent metal surface [127]. The PVD method has been used by the Kyriakou group for the development of the Pd/Cu(111) SAA catalyst, who found that Pd atoms were predominantly placed above the step edges throughout terraces and areas with arbitrary dispersion [128]. Lucci and colleagues also produced Pd–Au SAAs

using a PVD technique for H₂ activation, and Pd–Au SAAs were shown to be beneficial for enhancing the CO tolerance of the catalysts [129]. Similarly, Hannagan et al. reported a similar conclusion on a RhCu/SiO₂ SAA in the dehydrogenation of propane, demonstrated through scanning tunnelling microscopy (STM) analysis, which showed an outlying Rh atom in Cu(111) [130]. In addition, temperature-programmed desorption analysis (TPD) was performed on Cu(111), sputtered Cu(111), 0.2% RhCu(111) SAA, and 0.2% RhCu(111) SAA; it was demonstrated that the RhCu/SiO₂ SAA had the highest propene selectivity (100%) [130].

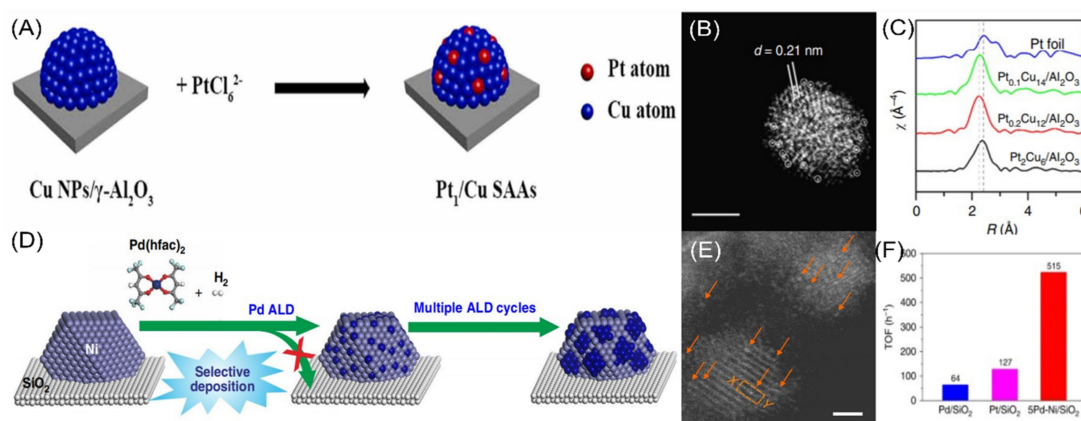


Figure 6. (A) Schematic description of GR method to synthesise Pt₁/Cu SAA NPs, (B) HAADF-STEM images of secluded Pt atoms with Cu metal particles using 2nm scale, and (C) EXAFS data at room temperature from Pt foil and pre-reduced Pt_{0.1}Cu₁₄/Al₂O₃, Pt_{0.2}Cu₁₂/Al₂O₃, and Pt₂Cu₆/Al₂O₃. Adapted with permission from [122], (D) schematic flow for the development of Pd₁Ni SAAs via ALD approach, (E) HAADF-STEM image for 5Pd-Ni/SiO₂ using 2 nm scale, and (F) the number of turnover frequencies (reaction parameter = 0.5 g catalyst loading under 0.6 MPa H₂ pressure at 80 °C). Adapted with permission from [131].

The ALD method is equally effective for SAA catalyst creation. As illustrated in Figure 6D, Wang and co-workers effectively produced a Pd₁Ni SAA for the hydrogenation of nitriles [131]. The HAADF-STEM images revealed a single Pd atom isolated on Ni NPs (Figure 6E). Acrolein hydrogenation over Pd₁Ni SAA was also found to be catalytic reactive. The turnover frequencies (TOFs) of the reaction over Pd/SiO₂ SAA, Pt/SiO₂ SAA, and 5PdNi/SiO₂ SAA (5% Pd is the best Pd concentration) were also determined. As expected, the TOF value of 5Pd-Ni/SiO₂ SAA was higher (515 h⁻¹) than that of Pd/SiO₂ (64 h⁻¹) and Pt/SiO₂ (127 h⁻¹) (Figure 6F). A two-step sequential reduction process was also introduced to produce complex SAA structures. This was demonstrated by Pei et al. [132] and Trimpalis et. al. [133] when they synthesised a Pd₁/Au SAA supported on silica gel for hydrogenation reactions and Ni_{0.005}Au/SiO₂ SAAs for selective oxidations of methacrolein. Furthermore, Yao and colleagues established a number of catalysts on a carbon support using this technique for water oxidation electrocatalysts, yielding catalysts with stable activity [134].

5.2. Top-Down Synthesis Strategies of SACs and SAAs

Besides the bottom-up strategy, SACs and SAAs have also been widely synthesised by top-down synthetic methods via the high temperature pyrolysis method, the high temperature metal migration method, and the ball-milling process. These approaches have been shown to be capable of generating SACs with precise frameworks, easy scalability, and high metal loading [135]. The disintegration of organised nanostructures into smaller bits is described as a top-down technique. This technique has proven to be particularly effective in the creation of SACs with a high precision over microstructures or nanomaterials [136]. The high temperature pyrolysis method has been a prominent way to synthesise nanosized carbon-supported SACs. This method appears to include the construction of a template-

sacrificial approach by acid leaching or calcination at temperatures ranging from 400 to 600 °C [137–140]. Li and colleagues proved this strategy in the synthesis of Zn–N–C SACs and Fe–N–C SACs using ZnCl₂ and FeCl₃·6H₂O as a precursor for the ORR process, and the findings of XANES and EXAFS tests demonstrated that Zn–N₄ and Fe–N₄ were the main active sites in the Zn–N–C SACs and Fe–N–C SACs [141]. As demonstrated by the DFT calculations, the Zn–N₄ structure is more electrochemically robust than the Fe–N₄ structure in Fe–N–C during the ORR process, owing to Zn's full-filled d-orbital (3d₁₀4s₂) greater free energy. Yin and colleagues also used a high temperature pyrolysis method at 800 °C for the development of a CoSAs/N–C catalyst for ORR [142]. The result showed that CoSAs/N–C (900) exhibited the most elevated ORR action over CoNPs/N–C and commercial Pt/C catalysts. Zhao et al. prepared Ni SAs/N–C and Ni NPs/N–C using Zn nodes as ionic transfer and the adsorbed Ni salts method at 1000 °C; the results demonstrated the Ni SAs/N–C catalyst has a higher value of onset potential for reversible hydrogen electrodes (RHEs) than the Ni NPs/N–C catalyst [143]. A higher onset potential is beneficial for CO₂ reduction due to a faster electron transfer rate at a given potential, thereby enhancing the reaction.

For synthesising SAA catalysts, a ball milling method has been reported to be an effective approach [48,144,145]. This method can disrupt and rebuild the chemical bonds in materials or molecules with an appropriate energy input. As reported by Deng and co-workers [48] in the synthesis study of GN-embedded FeN₄ (FeN₄/GN) catalysts via ball milling, this catalyst exhibited an 18.7% phenol yield with a conversion of 23.4% for the direct catalytic oxidation of benzene to phenol. The high stability of the FeN₄/GN catalyst was proven by yielding 8.3% of phenol after 24 h of reaction time. The catalytic activity in the GN matrix was found to be positively influenced by the highly dispersed and well-stable FeN₄ centres. Gan et al. used the ball milling technique in the synthesis of Pt₁/Co SAAs for the hydrodeoxygenation (HDO) reaction of 5-hydroxymethylfurfural (HMF) to 2,5-dimethylfuran (DMF). The results illustrated that the catalyst obtained high HMF conversion (100%) and was highly selective towards DMF (93%) [144]. A similar method was used by Gan et al. for the development of Au₁/CeO₂ SAAs for the preferential oxidation of CO [145]. They found that Au₁/CeO₂ SAAs showed an excellent stability and superior activity by converting 100% of CO after 160 h in stream. Even though SAA catalysts have been shown to be useful for several reaction activities, the top-down manufacturing technique for SAAs has received little attention.

Table 2 shows the merits and downsides of the various SAC and SAA synthesis approaches. Although PVD appears to be successful for the activation and desorption of reactants in theory, it is not suited for practical use due to the high equipment cost and low yield. Notably, because of its ability to control particle size and dispersion, ALD is commonly used for the large-scale synthesis of stable SACs and SAAs. However, the ALD process has certain limitations, such as slow deposition rates and a shortage of metal precursors. The incipient wetness co-impregnation process is simple and widely acknowledged amongst the most cost-effective methods for manufacturing SACs and SAAs in the enterprise environment. Due to the inclusion of single metal atoms in NPs, this approach cannot be employed for large metal loadings surpassing 1 wt.%. Following that, GR can introduce many different types of SAC and SAA structures, but it is limited to specific differences in reduction potentials between the two metals, whereas the sequential reduction method has the advantage of employing SACs outside of the metal host via segregated reduction, though the process is somewhat difficult. Finally, the ball milling process has been versatile and suitable for the large-scale production of SAAs, but due to its limitations in terms of time and high equipment cost, this method is also not favoured. To summarise, using the wet-chemical route, specifically wetness co-impregnation and sequential reduction, is more preferred in the production of SACs and SAAs due to their low cost and being the easiest method to prepare, along with varying metal atom choices.

Table 2. Synthetic method of bottom-up and top-down strategies for SACs and SAAs catalysts.

Method	Merits	Demerits	Catalysts	Application	Performance/Condition	Ref.
<i>Bottom-up strategy</i>						
Atomic layer deposition (ALD)	Controllable size and dispersion of particles	High equipment cost Low yield	Pt/graphene SAC	Methanol oxidation	Pt/graphene SAC found to be effective for methanol oxidation at 0.59, 0.60, 0.62, and 0.7 V with order of ALD cycles 50–150.	[114]
			Pd ₁ Ni SAA	Hydrogenation	Successful hydrogenolysis of nitriles by Pd/Ni to secondary amines with yield > 94%, exhibiting excellent recyclability.	[131]
Physical vapour deposition (PVD)	Simple preparation	High equipment cost Low yield	Pd-Au SAAs	Hydrogenation	Pd–Au SAAs highly dissociate H ₂ at 85 K, and reaction better than that of Au (111).	[129]
			RhCu/SiO ₂ SAA	Dehydrogenation	RhCu/SiO ₂ SAA catalyst showed propene selectivity 100% versus ~80% on Pt/Al ₂ O ₃ and sustained transformation of propane to propene and hydrogen for more than 50 h on stream at 623 K.	[130]
Co-precipitation	Simple and quick preparation Low cost	Easy agglomeration Low metal loading	Au ₁ /CeO ₂ SAC and Au ₁ /FeO _x SAC	Preferential oxidation of CO	Au ₁ /CeO ₂ SAC and Au ₁ /FeO _x SAC effectively catalysed CO conversion at 60–90 °C with excellent stability.	[115]
			Pt ₁ /ZnO SAC and Au ₁ /ZnO SAC	Methanol steam reforming (MSR)	Pt ₁ /ZnO SAC catalyst showed 43% conversion at the steady state, higher than that of Au ₁ /ZnO SAC (28%). Au ₁ /ZnO SAC showed higher CO ₂ selectivity (100%) than Pt ₁ /ZnO (88%).	[116]
			Ir ₁ /FeO _x SAC	Water–gas shift (WGS)	Under atmospheric pressure with different Ir loadings from 0.01, 0.22, 0.32, and 2.40, the Ir ₁ /FeO _x SAC showed high WGS activity.	[86]
Incipient wetness co-impregnation	Low cost Simplest method Varies metal choices	Low yield	Pd-Ag/SiO ₂ _SeqIWI SAA and Pd-Ag/SiO ₂ _CoIWI SAA	Hydrogenation	Pd atom enhances acrolein adsorption through the C=C bond (1.36 eV) more dramatically than the C=O bond while acrolein adsorbs weakly to the monometallic pure Ag/SiO ₂ catalyst.	[125]
			Pt ₁ /ATO (antimony doped tin-oxide) SAA	Electrochemical reactions—formic acid oxidation reaction (FAOR)	Owing to the existence of single atomic Pt sites, which initiate the O–H bond of formic acid and have good resistance, the Pt ₁ /ATO SAA catalyst exhibited superior FAOR activity.	[126]
Sequential reduction	Available complex structure	Complicated steps Uncontrollable structure	Ni _{0.005} Au/SiO ₂ SAA	Selective oxidation	Ni _{0.005} Au/SiO ₂ SAA showed superior activity with 100% conversion to methyl methacrylate (MMA) than NiAu/SiO ₂ (2%) for selective oxidation of methacrolein with methanol to MMA.	[133]
			Ru ₁ –PtCu ₃ /AC SAA, Ru ₁ –PtCu/AC SAA, and Ru ₁ –Pt ₃ Cu/AC SAA	Water oxidation Electrocatalysis	The PtCu alloy's OER activity was low, with an oxidation potential of 410, implying that the atomically scattered Ru ₁ incorporated into the Pt–Cu alloys serve as, or at least participate in, the OER active sites.	[134]

Table 2. Cont.

Method	Merits	Demerits	Catalysts	Application	Performance/Condition	Ref.
Galvanic replacement	Special compositions and structures	Need difference reduction potential between two metals Limited choices	Pd ₁ Cu SAA, Pt ₁ Cu SAA, and NiCu SAA.	Ethanol dehydrogenation	NiCu SAA alloy exhibited higher activity than Pd ₁ Cu SAA and Pt ₁ Cu SAA due to the presence of Ni, which lowers the barrier for C–H activation and thus increases the activity.	[120]
			Pt/Cu SAAs	C–H activation	Catalytic studies showed that Pt/Cu SAAs catalysed the exchange reaction at 250 °C, compared to ~550 °C on Cu NPs, and are stable during the reaction.	[121]
			Pt/Cu SAAs'	Hydrogenation	Near 2D volcano plot, Ru ₁ –Pt ₃ Cu (111) showed the highest OER activity ($\eta = 0.42$ V) while Ru ₁ –Cu (111), Ru ₁ –PtCu ₃ (111), Ru ₁ –PtCu(111), and Ru ₁ –Pt (111) exhibited 0.82, 0.71 and 0.66, and 0.92 V, respectively, which are less dynamic.	[122]
<i>Top-down strategy</i>						
High-temperature pyrolysis	Suitable large-scale production Easy to anchor heteroatoms	Dangerous etching (HF) High temperature needed	Co SAs/N-C, Co NPs-N/C, and Pt/C	Electroreduction of CO ₂	CoSAs/N–C (900) had the strongest ORR activity, with an E _{onset} number that was almost comparable to Pt/C (0.982 V vs. RHE) and E _{1/2} (0.881 V) more favorable than that of Pt/C (0.811 V) and CoSAs/N–C (800) (0.863 V).	[142]
			Ni SAs/N-C and Ni NPs/N-C	Electroreduction of CO ₂	Ni SAs/N–C catalyst demonstrated higher amount of onset potential for reversible hydrogen electrode (RHE) than Ni NPs/N–C catalyst.	[143]
Ball milling	Easy scalable Environmentally friendly	High maintenance Time consuming	FeN ₄ /GN SAAs	Catalytic oxidation benzene to phenol	FeN ₄ /GN showed phenol yield (18.7%) and conversion (23.4%) for direct catalytic oxidation of benzene to phenol. The FeN ₄ /GN also exhibited high stability by yielding 8.3% of phenol after 24 h of reaction time.	[48]
			Pt ₁ /Co SAAs	Hydrodeoxygenation	Pt ₁ /Co SAAs showed high HMF conversion (100%) and were highly selective towards DMF (93%) for the catalyst.	[144]
			Au ₁ /CeO ₂ SAAs	Preferential oxidation of CO	Au ₁ /CeO ₂ SAAs had 100% CO conversion after 160 h in the mainstream, showing that the catalyst has excellent stability and superior activity.	[145]

6. The Challenge and Opportunities of SACs and SAAs in Biofuel Production

In recent years, there has been a lot of interest in SACs and SAAs for biofuel. With all the benefits discussed above, the utilisation of these catalysts, especially in liquid-phase reactions, is still problematic because of their stability issues [21]. The mass loading of SACs and SAAs is also one of the reasons for limiting the overall production rate in the reaction system. Increasing the precursor concentration during the synthesis of SACs and SAAs will not fix these problems since the strong metal–metal interactions will cause single atoms to form metal clusters or nanoparticles. Figure 7A provides the annual number of scholarly works on SACs. In recent years, fewer scholarly works were found for biofuel processes using SACs. Most of the work was published in scientific journals, with a total of 630 publications from 2000 to 2022. The result also revealed that the application of SACs in biofuel showed remarkable growth from 2011 to 2020, and globally, this research attained its highest peak level in 2017. Elsevier is of note as a significant publisher of topics surrounding the use of SACs for biofuel (Figure 7B).

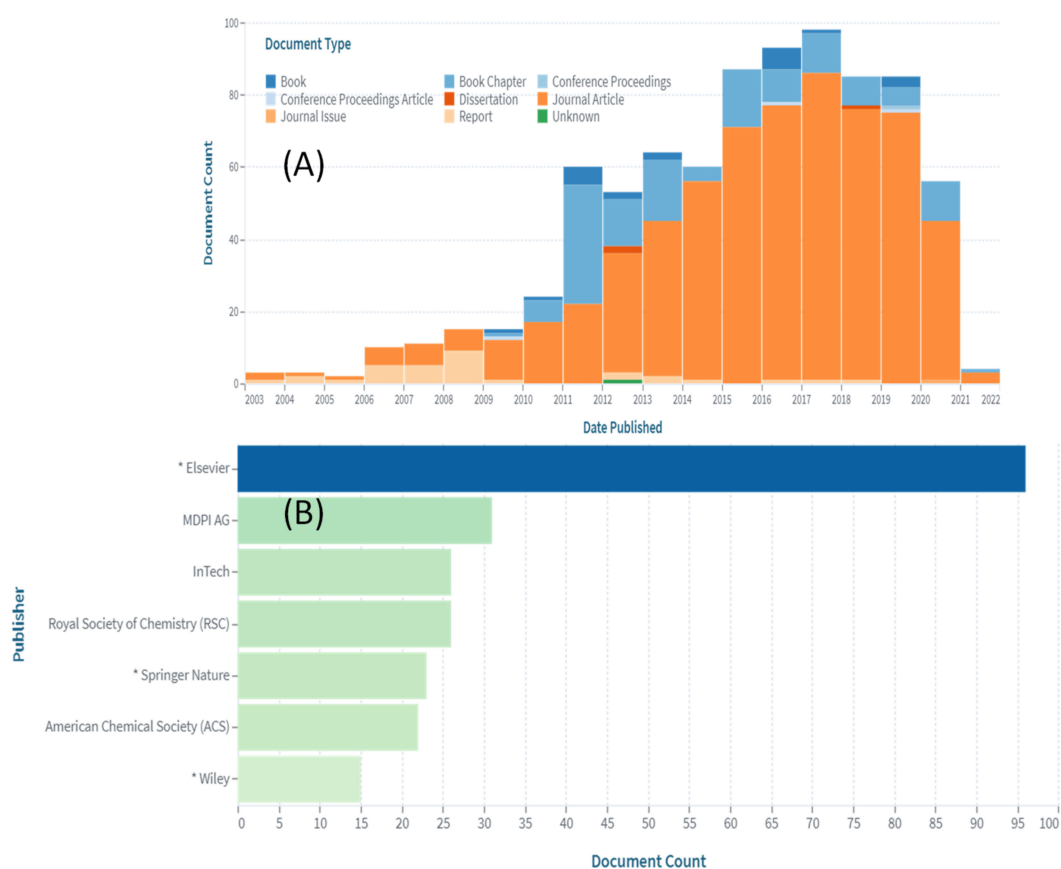


Figure 7. (A) The annual number of scholarly works on SACs and biofuel and (B) scholarly work on SAC and biofuel (published by top 5 publishers). (The Lens (formerly Patent Lens) scholar analysis search system, search term “single-atom-catalyst AND biofuel” within 2000–2021). <https://link.lens.org/LXnxsRHrG9c> (accessed 11 October 2021). * The annual number of scholarly works on SACs and biofuel.

Table 3 shows recent studies focused on the utilisation of SACs and SAAs in renewable chemical and biofuel (liquid and gas) production processes. In summary, the biofuel production process over SACs and SAA catalysts has been extensively investigated at the atomic level, in which most of the catalysts focus on the production of gas biofuels (hydrogen) from biomass and gas phases; the production of liquid biofuel over SACs has also been conducted, but it is insignificant or minor. An example in this regard is shown in the work by Liu et al. [146], in which they used Co-MoS₂ SAC in the hydrodeoxygenation of biomass 4-methylphenol at 180 °C to toluene. Compared with traditional Co/MoS₂

catalysts, Co-MoS₂ SAC showed a higher selectivity, activity, and stability. This study also revealed that a large number of basal sulphur vacancies within Co-doped single-layer MoS₂ provided a sufficient number of Co-S-Mo active sites for the hydrodeoxygenation reaction to occur at a low operating temperature. Later in the same year, Cao and co-workers reported on the hydrogenation of biomass levulinic acid (LA) to (renewable chemicals and fuels: γ -valerolactone (GVL)) over 0.85 wt.% of Ru/ZrO₂@C SAC catalyst using a new stabilisation strategy based on UiO-66 (Zr-MOF) material [147]. There was no reduction in catalytic performance after recycling. There was also no leaching of ruthenium found even under pH 1. Compared with commercial Ru/C, which is highly active and selective, the downside is that it undergoes severe deactivation due to Ru leaching. Recently, the transformation of liquid biomass (castor oil) to a liquid biofuel (octadecane) over Fe-Au-Pd SAAs via hydrodeoxygenation in 3 h at 250 °C, 40 bar of H₂, and 20 bar of CO₂ pressure was reported by Bhattacharjee et al., and the result revealed that the octadecane selectivity was obtained at 72.6% [148]. Indeed, it can be seen that most of the SACs and SAA catalysts demonstrate remarkable stability with excellent catalytic activity compared to traditional catalysts, which often require harsher reaction conditions, such as elevated hydrogen pressure, moderate to high reaction temperatures, and hot water or even acidic reaction media.

Apart from studies related to the transformation of biomass into liquid chemicals or biofuels, there have been many studies reported on the production of gas biofuel hydrogen. Firstly, the study by Akri and co-workers showed that Ni SACs are effective in the DRM reaction and allow carbon deposition to react with CO₂ at 750 °C to syngas (CO, H₂), which is an indication of having an excellent resistance to carbon deposition [149]. Using the strong electrostatic adsorption (SEA) approach, Akri's group was able to easily synthesise single-atom Ni nanoparticle dispersed on a hydroxyapatite (HAP) substrate. The experiments showed that Ni SACs demonstrate a significant improvement in stability when polyvinylpyrrolidone (PVP) is used in preparing the catalyst. It is worthy of mention that the efficacy of SACs to be used in high-temperature reactions has been confirmed.

Formaldehyde oxidation and photocatalytic hydrogen synthesis (solar-driven hydrogen evolution) on the ultrathin carbon nitride (SAVCN) with a charge-transfer on the V-N bridge as the reaction switch has also been recently characterised [150]. Surprisingly, the V-N bridge's electronic structure enables the photocatalytic hydrogen evolution activity to be nearly three times that of virgin carbon nitride. Jin and co-authors discovered that bringing the most common unpaired d-electron in the photocatalyst into the intermediate state by modifying the oxidation state of Ni single-atom active sites to a specific Ni²⁺/Ni⁰ ratio optimises the electronic production for dramatically improved photocatalytic performance [151]. As a result, the photocatalytic hydrogen generation rate approached 354.9 $\mu\text{mol h}^{-1} \text{g}^{-1}$, which is among the highest reported for carbon nitride photocatalysts ornamented with single metal atoms, especially low-cost transition-metal single atoms.

Zhang and co-authors recognised that the fixed bond and oxidation state should be extremely simple in single-atom Pt/C₃N₄ SAC photocatalysts; the dynamic electron transfer and bond changes between the single-atom Pt and C₃N₄ were first demonstrated by combining SI-XPS and SI-DRIFTS after light irradiation [152]. Pt⁰ and C₃N₄ are designated as sites for reduction and oxidation reactions, respectively, by the bond evolution. As a result, single-atom Pt/C₃N₄ SAC has a much better photocatalytic H₂ evolution performance than Pt particle-C₃N₄ and C₃N₄. Indeed, Zhou et al. discovered a similar trend in photocatalytic activity at sub-zero temperatures over PtNP-loaded g-C₃N₄SAC catalysts [153], with the findings indicating that H₂ evolution was particularly successful due to a reactive metal-support interaction (RMSI). Trofimovaite et al., who studied photocatalytic activity over Cu/meso-TiO₂-500C SAC, state that with a controllable pattern, photophysical specifications and high surface area properties play an important factor in improving the photocatalytic activity [154].

There are few studies reported on the production of hydrogen via WGS reactions [155,156]. Liang et al. [155] reported a combined theoretical and experimen-

tal single-atom Ir₁/FeO_x study of the WGS reaction on an Ir₁/FeO_x catalyst. It was shown that the dual metal active site consisting of Fe and Ir₁ single atoms has a synergetic effect to catalyse the WGS reaction with the involvement of an oxygen vacancy (O_{vac}) on the surface of Ir₁/FeO_x. This work further supports the concept that for SACs, covalent metal–support interaction plays a unique role in tuning their catalytic properties and also supports the role of Ir₁ single atoms in stabilising the catalyst in the form of the Ir–O–Fe moiety, which plays a dominant role in the WGS reaction. Interestingly, the SACs were also found to be effective in WGS at room temperature. This was evinced by Li and her co-workers [156] in the WGS reaction over single-atom nanocatalyst Pt@Mo₂C. Notably, WGS activity over Pt@Mo₂C SAC was found to be similar to that of the Pt systems, implying the advantage of lower cost.

It has been well-established by the previous section that hydrogen generation can be efficiently produced via CO₂RR. The effectiveness of SACs was strongly confirmed by a recent finding using a single-atom CoNi-NC catalyst [157]. The CoNi-NC was discovered to be advantageous in balancing CO₂RR activity and producing high yields of CO and H₂. A series of Co and Ni concentrations were studied in order to tune the CO/H₂ ratio suitable for use in thermochemical reactions, and it was concluded that varying the Ni and Co ratio in CoNi-NC represents an opportunity to further tune the CO/H₂ ratio without sacrificing the high syngas production rate. Last but not least, SACs have been employed in the semi-hydrogenation of acetylene to produce ethylene gas [158]. Surprisingly, the Cu alloyed Pd SAC demonstrated an ~85% selectivity for ethylene and 100% removal of acetylene. The Cu alloyed analog's conversion outperformed both the Au and Ag alloyed Pd SACs, while its selectivity was on par with the Ag alloyed Pd SAC and even better than the Au alloyed Pd SAC.

Based on Table 3, it can be seen that SACs and SAAs are very effective for the conversion of biomass, organic chemicals, and GHGs (CO₂, CO) to biofuel under various reaction temperatures (room temperature to > 300 °C). It is worth noting that research on high-temperature reactions are limited in number. Contradicted with the reaction at room temperature, in which UV-light is used as a source, transformation of UV-light to gas biofuel at a lower reaction temperature via photocatalytic water splitting, dye degradation, and electrochemical CO₂RR, have been researched in numerous studies [150,151,154,157]. Based on the above finding, the high effectiveness of SACs and SAAs in photocatalytic reactions is owing to their electron configuration, which apparently results in an elevated light response, conductivity, charge separation, and mobility of the photocatalyst [151]. Similarly, a single-atom configuration is beneficial for an increment of total current density, which consequently leads to optimal metal catalyst utilisation and improves the electro/thermocatalytic processes for CO₂RR [157]. In the case of biomass transformation at high reaction temperatures, SACs and SAAs, which have a maximum atomic efficiency and a uniform and tunable metal centre, as well as an adjustable metal–support interaction, were the keys to boosting the catalyst efficiency and thermal stability. Their well-defined and uniform structure also provides advantages to fundamental studies for understanding the intrinsic reaction mechanism and site requirement in biomass and CO₂ conversion [159].

Other than liquid biofuel and gas biofuel processes, SACs and SAAs have recently shown great promise for environmental catalysis against a variety of pollutants due to the maximum site exposure by SACs and SAAs. It should be noted that SACs and SAAs can also be used effectively for major reactions such as the electrochemical oxidation of volatile organic compounds (VOCs), dehydrogenation of VOCs, and SO₃ decomposition [160,161].

Table 3. Summarisation of SACs and SAAs in the production of biofuel and renewable chemicals.

Catalyst/ Biofuel and Renewable Chemical	Reaction	Product	Remarks	Refs.
<i>Liquid renewable chemicals/biofuels</i>				
Co–MoS ₂ SAC	Hydrodeoxygenation	Toluene Hydrocarbon fuels	-High metal dispersion and stability associated to a strong interaction between Ru and nano tetragonal ZrO ₂ . -The catalyst exhibited clear deactivation in the recyclability study. The deactivation of the catalyst was associated to the leaching.	[146]
Ru/ZrO ₂ @C SAC	Hydrogenation of levulinic acid (LA) to γ -valerolactone (GVL)	γ -valerolactone (GVL)	-A strong covalent bond between Co atoms to monolayer MoS ₂ enhances the number of Co–S–Mo interfacial. -The catalyst is clearly effective and highly stable for 4-methylphenol to toluene transformation.	[147]
Fe–Au–Pd SAAs	Hydrodeoxygenation	Octadecane	Octadecane selectivity of 76% was obtained.	[148]
<i>Gas biofuel</i>				
Ni SACs	Dry methane reforming (DRM)	Carbon monoxide and hydrogen	-Ni SACs is coking-resistant agent. -PVP method during catalyst synthesis stabilised the catalyst.	[149]
SAVCN SAC	Photocatalytic hydrogen production and formaldehyde oxidation	Hydrogen	-SAVCN rendered excellent photo-catalytic activity at room temperature.	[150]
CN–0.2Ni–HO (CN: nitride)	Photocatalytic water splitting	Hydrogen	-Photocatalytic H ₂ production rate was the highest (354.9 $\mu\text{mol h}^{-1} \text{g}^{-1}$), higher than that of reported CN photocatalysts SACs.	[151]
Pt–C ₃ N ₄ SAC	Photocatalytic water splitting	Hydrogen	-High H ₂ production activity (14.7 $\text{mmol}\cdot\text{h}^{-1}\cdot\text{g}^{-1}$) was achieved over Pt/C ₃ N ₄ SAC catalyst.	[152]
PtNP-loaded g–C ₃ N ₄ SAC	In situ photocatalytic reduction method at a sub-zero temperature	Hydrogen	The reaction activity was 20 times higher than that of metallic Pt–C ₃ N ₄ catalyst. -Excellent H ₂ evolution is due to RMSI. -RMSI contributes to the supra-high-density PtSAs on the electron-deficient g–C ₃ N ₄ .	[153]
Cu/meso–TiO ₂ –500C SAC	Photocatalytic dye degradation	Hydrogen	-A synergy between Cu(I) and CuO increased photocatalytic H ₂ production four-fold relative to the mesoporous anatase scaffold. -Tailoring textural and photophysical properties positively affect chemical mass transport, energetics, and lifetime of charge carriers.	[154]
CoNi–NC SAC	The electrochemical CO ₂ reduction reaction (CO ₂ RR)	Hydrogen, carbon monoxide	-The CoNi–NC catalysts maintained the high syngas yield.	[157]
Ir ₁ /FeO _x SAC	Water–gas shift	Hydrogen	-Co and Ni with varies ratios co-existed in an SAC configuration exhibited to have controllable CO/H ₂ ratios.	[155]
Pt@Mo ₂ C SAC	Water–gas shift	Hydrogen	-Fe and Ir ₁ single atoms play a synergetic effect to catalyse the WGS reaction. -Pt@Mo ₂ C SAC promoted WGS, demonstrating the advantages of lower cost and higher thermal stability.	[156]
Cu alloyed Pd SAC	Semi-hydrogenation of acetylene	Ethylene	-The synergetic effect of bimetallic (Mo–Pt) is beneficial to H ₂ production. -Ethylene selectivity of ~85% was achieved. -The isolation of Pd atoms by the IB metal played a key role in enhancing the ethylene selectivity, while the electronic effect had a relatively minor effect on their catalytic performances.	[158]

Based on the above discussion, despite tremendous advances in the synthesis and environmental catalysis of SACs and SAAs, there are still a number of challenges to overcome, which are detailed in the following section.

1. Large-scale and controllable SACs and SAAs preparation

The evolution of appropriate techniques to upscale SAA manufacture under moderated conditions is of value but remains a challenge for pragmatic functionality. Contemporary protocols for SAA synthesis have included PVD, ALD, and wet-chemistry processes. A number of hurdles still need to be surmounted in order to upscale SAA manufacture via a straightforward and widespread approach and to have an effective expenditure: yield ratio [162].

2. Stability of SACs and SAAs

The practical utility of SAAs mandates their stability, particularly for reactions over the long-term and at high temperatures. An issue is maintaining the single-atom properties over long-term employment owing to the marked inclination of the high surface energy to generate clustering. The lone atomic active loci of SAAs should thus be appraised by deploying in situ analytical techniques over the course of reactions. Of note is that choosing the alloy elements and enhancing their engagement has the potential to upgrade their stability [163].

3. Additional SACs and SAAs applications in the environmental sector

Contemporary studies have only concentrated on conventional contaminants, e.g., VOCs and additional noxious inorganic vapours [160]; there is little research evaluating the eradication of water pollutants [86]. From both experimental and pragmatic perspectives, SAAs have a lot of promise for the recovery of air, water, and soil. They are also likely to be of value for the extraction and conversion of VOCs through a range of catalytic pathways. For instance, VOCs can be efficaciously oxidised into water, CO₂, and additional non-toxic substances at low temperatures using catalytic oxidation. Thus, there is significant potential for the application of SAAs for diverse catalytic reactions in the environmental sector [86,161,164]

4. Complex SACs and SAAs structures for specific applications

Attention has been drawn to the synthesis of involved SAA configurations from SAA basic elements for targeted use. These constructs offer the individual traits of the SAA, whereas the complicated infrastructure yields a superior surface area with a plethora of active loci, improved porosity, and upgraded mass and electron transfer. Thus, the production of intricate SAA configurations with high performance statistics for certain utilities is an attractive proposition [165,166].

5. Further studies on the active sites and reaction mechanisms of SACs and SAAs

A more in-depth comprehension of active loci and reaction pathways is key to enhancing and designing efficacious catalysts. The transparent and regular configuration of SAAs enables the recognition of active loci and the delineation of mechanisms underlying the reactions via DFT computations, analytical methods, and catalytic appraisals. Nevertheless, during a reaction, SAA catalysts may be subject to a dynamic reconfiguration; in situ progressive analytical techniques should be employed in order to examine geometric reconformations of active loci during the catalysis. This would enable structure–property associations and reaction pathways to be characterised and facilitate the logical creation of efficacious catalysts [165].

An ongoing issue is generating a hypothetical model of sizeable and involved molecules using DFT simulation. Additional computations are necessary to assess the absorption and activation functionality of significant environmental contaminants with respect to SAA catalysts in order to comprehend the relevant catalytic pathways and screen for appropriate catalysts [167].

Despite the fact that SACs and SAAs face significant challenges in making them viable for a variety of important applications, such as high-temperature biofuel production pro-

cesses and electrochemical energy conversion, both of these catalysts show great promise in terms of metal utilisation, catalytic site tunability, and selectivity. It is noteworthy to mention that in the form of single atoms, they drastically reduced the catalyst cost. Active noble metals are costly; thus, the downsizing of noble metals from nanoclusters to isolated single atoms is an ideal strategy that will significantly reduce the cost and enhance the economic viability of each of the catalytic processes.

7. Conclusions and Remark

Years have passed since SACs and SAAs were first introduced, and there has been remarkable progress in the development of strategies to synthesise both SACs and SAAs. In this review paper, we have summarised the progress of synthetic methods of SACs and SAAs for various catalytic reactions and the new development methods that benefit the production of liquid and gas biofuels. Most of the synthetic methods used for the development of SACs and SAAs are wet-chemical routes, co-impregnation, and sequential reduction. As discussed previously, the challenge of synthesising SACs and SAAs in the liquid phase is their stability. Single atoms generally have high energy, so only when they are fixed on the support can they be stable. There are two strategies that can be used to overcome this challenge, which are mutual metal–support interaction and the coordination geometric effect. More, it has also been found that coordination number, nano-structuring, and ligand selection affect the catalytic activity of SACs and SAAs. Next, it is challenging to find a practical method to strongly anchor single atoms on high-surface area and low-cost support materials. There is only a small amount of research that has been done specifically for liquid biofuels. Further investigation of SACs and SAAs for liquid biofuel production is expected to have more innovative synthesis strategies, advanced characterisation tools, and theoretical calculations to understand the intrinsic properties of supported single-atom metals and catalytic systems to obtain a fascinating design of SACs and SAAs for desirable reactions with high efficiency and sustainability applications.

Author Contributions: Conceptualization, N.A.-M.; validation, N.A.-M., H.M.S. and H.C.O.; writing—original draft preparation, N.A.-M. and N.A.A. (Nurul Ahtirah Azman); writing—review and editing, N.A.-M., H.M.S., N.A.A. (Nur Athirah Adzahar) and A.G.A.; visualization, N.A.-M.; supervision, N.A.-M. and H.C.O.; funding acquisition, N.A.-M. and H.C.O. All authors have read and agreed to the published version of the manuscript.

Funding: This research was funded by Galakan Penyelidik Muda (GGPM) (GGPM-2020-015) and GP-2021-K023310.

Acknowledgments: The authors acknowledge the financial support from Galakan Penyelidik Muda (GGPM) (GGPM-2020-015) and GP-2021-K023310.

Conflicts of Interest: The authors declare no conflict of interest.

References

1. Xiong, X.; Yu, I.K.M.; Cao, L.; Tsang, D.C.W.; Zhang, S.; Ok, Y.S. A review of biochar-based catalysts for chemical synthesis, biofuel production, and pollution control. *Bioresour. Technol.* **2017**, *246*, 254–270. [[CrossRef](#)] [[PubMed](#)]
2. Thanh, L.T.; Okitsu, K.; Van Boi, L.; Maeda, Y. Catalytic technologies for biodiesel fuel production and utilization of glycerol: A review. *Catalysts* **2012**, *2*, 191–222. [[CrossRef](#)]
3. Cheng, F.; Li, X. Preparation and application of biochar-based catalysts for biofuel production. *Catalysts* **2018**, *8*, 346. [[CrossRef](#)]
4. Lee, R.A.; Lavoie, J.M.J.-M. From first- to third-generation biofuels: Challenges of producing a commodity from a biomass of increasing complexity. *Anim. Front.* **2013**, *3*, 6–11. [[CrossRef](#)]
5. Mohr, A.; Raman, S. Lessons from first generation biofuels and implications for the sustainability appraisal of second generation biofuels. *Effic. Sustain. Biofuel Prod. Environ. Land-Use Res.* **2015**, *63*, 281–310. [[CrossRef](#)]
6. Chandra, R.; Takeuchi, H.; Hasegawa, T. Methane production from lignocellulosic agricultural crop wastes: A review in context to second generation of biofuel production. *Renew. Sustain. Energy Rev.* **2012**, *16*, 1462–1476. [[CrossRef](#)]
7. Salama, E.S.; Kurade, M.B.; Abou-Shanab, R.A.I.; El-Dalatony, M.M.; Yang, I.S.; Min, B.; Jeon, B.H. Recent progress in microalgal biomass production coupled with wastewater treatment for biofuel generation. *Renew. Sustain. Energy Rev.* **2017**, *79*, 1189–1211. [[CrossRef](#)]

8. Dutta, K.; Daverey, A.; Lin, J.G. Evolution retrospective for alternative fuels: First to fourth generation. *Renew. Energy* **2014**, *69*, 114–122. [[CrossRef](#)]
9. Havlík, P.; Schneider, U.A.; Schmid, E.; Böttcher, H.; Fritz, S.; Skalský, R.; Aoki, K.; De Cara, S.; Kindermann, G.; Kraxner, F.; et al. Global land-use implications of first and second generation biofuel targets. *Energy Policy* **2011**, *39*, 5690–5702. [[CrossRef](#)]
10. Serrano, D.P.; Melero, J.A.; Morales, G.; Iglesias, J.; Pizarro, P. Progress in the design of zeolite catalysts for biomass conversion into biofuels and bio-based chemicals. *Catal. Rev. Sci. Eng.* **2018**, *60*, 1–70. [[CrossRef](#)]
11. Picazo-Espinosa, R.; Gonzalez-Lopez, J.; Manzaner, M. Bioresources for Third-Generation Biofuels. *Biofuel's Eng. Process Technol.* **2011**. [[CrossRef](#)]
12. Li, X.; Luo, X.; Jin, Y.; Li, J.; Zhang, H.; Zhang, A.; Xie, J. Heterogeneous sulfur-free hydrodeoxygenation catalysts for selectively upgrading the renewable bio-oils to second generation biofuels. *Renew. Sustain. Energy Rev.* **2018**, *82*, 3762–3797. [[CrossRef](#)]
13. Abdullah, S.H.Y.S.; Hanapi, N.H.M.; Azid, A.; Umar, R.; Juahir, H.; Khatoon, H.; Endut, A. A review of biomass-derived heterogeneous catalyst for a sustainable biodiesel production. *Renew. Sustain. Energy Rev.* **2017**, *70*, 1040–1051. [[CrossRef](#)]
14. Friend, C.M.; Xu, B. Heterogeneous catalysis: A central science for a sustainable future. *Acc. Chem. Res.* **2017**, *50*, 517–521. [[CrossRef](#)]
15. Pálínkó, I. *Heterogeneous Catalysis: A Fundamental Pillar of Sustainable Synthesis*; Elsevier Inc.: Amsterdam, The Netherlands, 2018; ISBN 9780128095492.
16. Lam, M.K.; Lee, K.T. Scale-Up and Commercialization of Algal Cultivation and Biofuel Production. In *Biofuels from Algae*; Elsevier B.V.: Amsterdam, The Netherlands, 2013; pp. 261–286. ISBN 9780444595584.
17. Thakuria, H.; Borah, B.M.; Das, G. Macroporous metal oxides as an efficient heterogeneous catalyst for various organic transformations-A comparative study. *J. Mol. Catal. A Chem.* **2007**, *274*, 1–10. [[CrossRef](#)]
18. Asikin Mijan, N.; Lee, H.V.; Abdulkareem Alsultan, G.; Afandi, A.; Taufiq-Yap, Y.H. Production of green diesel via cleaner catalytic deoxygenation of *Jatropha curcas* oil. *J. Clean. Prod.* **2017**, *167*, 1048–1059. [[CrossRef](#)]
19. Gates, B.C.; Flytzani-Stephanopoulos, M.; Dixon, D.A.; Katz, A. Atomically dispersed supported metal catalysts: Perspectives and suggestions for future research. *Catal. Sci. Technol.* **2017**, *7*, 4259–4275. [[CrossRef](#)]
20. Hannagan, R.T.; Giannakakis, G.; Flytzani-Stephanopoulos, M.; Sykes, E.C.H. Single-Atom Alloy Catalysis. *Chem. Rev.* **2020**, *120*, 12044–12088. [[CrossRef](#)]
21. Zhang, L.; Ren, Y.; Liu, W.; Wang, A.; Zhang, T. Single-atom catalyst: A rising star for green synthesis of fine chemicals. *Natl. Sci. Rev.* **2018**, *5*, 653–672. [[CrossRef](#)]
22. Mitchell, S.; Pérez-Ramírez, J. Single atom catalysis: A decade of stunning progress and the promise for a bright future. *Nat. Commun.* **2020**, *11*, 10–12. [[CrossRef](#)] [[PubMed](#)]
23. Zhang, T.; Walsh, A.G.; Yu, J.; Zhang, P. Single-atom alloy catalysts: Structural analysis, electronic properties and catalytic activities. *Chem. Soc. Rev.* **2021**, *50*, 569–588. [[CrossRef](#)]
24. Zhang, X.; Cui, G.; Feng, H.; Chen, L.; Wang, H.; Wang, B.; Zhang, X.; Zheng, L.; Hong, S.; Wei, M. Platinum–copper single atom alloy catalysts with high performance towards glycerol hydrogenolysis. *Nat. Commun.* **2019**, *10*, 5812. [[CrossRef](#)] [[PubMed](#)]
25. Cao, X.; Mirjalili, A.; Wheeler, J.; Xie, W.; Jang, B.W.L. Investigation of the preparation methodologies of Pd-Cu single atom alloy catalysts for selective hydrogenation of acetylene. *Front. Chem. Sci. Eng.* **2015**, *9*, 442–449. [[CrossRef](#)]
26. Xing, F.; Jeon, J.; Toyao, T.; Shimizu, K.I.; Furukawa, S. A Cu-Pd single-atom alloy catalyst for highly efficient NO reduction. *Chem. Sci.* **2019**, *10*, 8292–8298. [[CrossRef](#)]
27. Zhang, L.; Liu, H.; Liu, S.; Norouzi Banis, M.; Song, Z.; Li, J.; Yang, L.; Markiewicz, M.; Zhao, Y.; Li, R.; et al. Pt/Pd Single-Atom Alloys as Highly Active Electrochemical Catalysts and the Origin of Enhanced Activity. *ACS Catal.* **2019**, *9*, 9350–9358. [[CrossRef](#)]
28. Huang, L.; Zhang, H.; Cheng, Y.; Sun, Q.; Gan, T.; He, Q.; He, X.; Ji, H. Quasi-continuous synthesis of cobalt single atom catalysts for transfer hydrogenation of quinoline. *Chin. Chem. Lett.* **2021**. [[CrossRef](#)]
29. Fei, H.; Dong, J.; Chen, D.; Hu, T.; Duan, X.; Shaker, I.; Huang, Y.; Duan, X. Single atom electrocatalysts supported on graphene or graphene-like carbons. *Chem. Soc. Rev.* **2019**, *48*, 5207–5241. [[CrossRef](#)] [[PubMed](#)]
30. Qin, R.; Liu, P.; Fu, G.; Zheng, N. Strategies for Stabilizing Atomically Dispersed Metal Catalysts. *Small Methods* **2018**, *2*, 1700286. [[CrossRef](#)]
31. Janampelli, S.; Darbha, S. Effect of support on the catalytic activity of WO_x-promoted Pt in green diesel production. *Mol. Catal.* **2018**, *451*, 125–134. [[CrossRef](#)]
32. Gamal, M.S.; Asikin-Mijan, N.; Arumugam, M.; Rashid, U.; Taufiq-yaq, Y.H.; Safa Gamal, M.; Asikin-Mijan, N.; Arumugam, M.; Rashid, U.; Taufiq-Yap, Y.H. Solvent-free catalytic deoxygenation of palm fatty acid distillate over cobalt and manganese supported on activated carbon originating from waste coconut shell. *J. Anal. Appl. Pyrolysis* **2019**, *144*, 104690. [[CrossRef](#)]
33. Khalit, W.N.A.W.; Asikin-Mijan, N.; Marliza, T.S.; Gamal, M.S.; Shamsuddin, M.R.; Saiman, M.I.; Taufiq-Yap, Y.H. Catalytic deoxygenation of waste cooking oil utilizing nickel oxide catalysts over various supports to produce renewable diesel fuel. *Biomass Bioenergy* **2021**, *154*, 106248. [[CrossRef](#)]
34. Lai, W.H.; Miao, Z.; Wang, Y.X.; Wang, J.Z.; Chou, S.L.; Qiao, B.; Wang, A.; Yang, X.; Allard, L.F.; Jiang, Z.; et al. Atomic-Local Environments of Single-Atom Catalysts: Synthesis, Electronic Structure, and Activity. *Adv. Energy Mater.* **2019**, *9*, 1900722. [[CrossRef](#)]
35. Qiao, B.; Wang, A.; Yang, X.; Allard, L.F.; Jiang, Z.; Cui, Y.; Liu, J.; Li, J.; Zhang, T. Single-atom catalysis of CO oxidation using Pt₁/FeO_x. *Nat. Chem.* **2011**, *3*, 634–641. [[CrossRef](#)] [[PubMed](#)]

36. Liu, J. Catalysis by Supported Single Metal Atoms. *ACS Catal.* **2017**, *7*, 34–59. [[CrossRef](#)]
37. Meng, G.; Zhang, J.; Li, X.; Wang, D.; Li, Y. Electronic structure regulations of single-atom site catalysts and their effects on the electrocatalytic performances. *Appl. Phys. Rev.* **2021**, *8*, 021321. [[CrossRef](#)]
38. Ren, Y.; Tang, Y.; Zhang, L.; Liu, X.; Li, L.; Miao, S.; Sheng Su, D.; Wang, A.; Li, J.; Zhang, T. Unraveling the coordination structure-performance relationship in Pt₁/Fe₂O₃ single-atom catalyst. *Nat. Commun.* **2019**, *10*, 4500. [[CrossRef](#)] [[PubMed](#)]
39. Greiner, M.T.; Jones, T.E.; Beeg, S.; Zwiener, L.; Scherzer, M.; Girgsdies, F.; Piccinin, S.; Armbrüster, M.; Knop-Gericke, A.; Schlögl, R. Free-atom-like d states in single-atom alloy catalysts. *Nat. Chem.* **2018**, *10*, 1008–1015. [[CrossRef](#)]
40. Thirumalai, H.; Kitchin, J.R. Investigating the Reactivity of Single Atom Alloys Using Density Functional Theory. *Top. Catal.* **2018**, *61*, 462–474. [[CrossRef](#)]
41. Chen, Y.; Huang, Z.; Ma, Z.; Chen, J.; Tang, X. Fabrication, characterization, and stability of supported single-atom catalysts. *Catal. Sci. Technol.* **2017**, *7*, 4250–4258. [[CrossRef](#)]
42. Kim, Y.T.; Ohshima, K.; Higashimine, K.; Uruga, T.; Takata, M.; Suematsu, H.; Mitani, T. Fine size control of platinum on carbon nanotubes: From single atoms to clusters. *Angew. Chem. Int. Ed.* **2006**, *45*, 407–411. [[CrossRef](#)] [[PubMed](#)]
43. Tauster, S.J.; Fung, S.C.; Garten, R.L. Strong Metal-Support Interactions. Group 8 Noble Metals Supported on TiO₂. *J. Am. Chem. Soc.* **1978**, *100*, 170–175. [[CrossRef](#)]
44. Tauster, S.J.; Fung, S.C.; Baker, R.T.K.; Horsley, J.A. Strong interactions in supported-metal catalysts. *Science (80-)* **1981**, *211*, 1121–1125. [[CrossRef](#)] [[PubMed](#)]
45. An, K.; Alayoglu, S.; Musselwhite, N.; Plamthottam, S.; Melaet, G.; Lindeman, A.E.; Somorjai, G.A. Enhanced CO oxidation rates at the interface of mesoporous oxides and Pt nanoparticles. *J. Am. Chem. Soc.* **2013**, *135*, 16689–16696. [[CrossRef](#)]
46. An, N.; Li, S.; Duchesne, P.N.; Wu, P.; Zhang, W.; Lee, J.F.; Cheng, S.; Zhang, P.; Jia, M.; Zhang, W. Size effects of platinum colloid particles on the structure and CO oxidation properties of supported Pt/Fe₂O₃ catalysts. *J. Phys. Chem. C* **2013**, *117*, 21254–21262. [[CrossRef](#)]
47. Najafshirtari, S.; Guardia, P.; Scarpellini, A.; Prato, M.; Marras, S.; Manna, L.; Colombo, M. The effect of Au domain size on the CO oxidation catalytic activity of colloidal Au-FeOx dumbbell-like heterodimers. *J. Catal.* **2016**, *338*, 115–123. [[CrossRef](#)]
48. Deng, D.; Chen, X.; Yu, L.; Wu, X.; Liu, Q.; Liu, Y.; Yang, H.; Tian, H.; Hu, Y.; Du, P.; et al. A single iron site confined in a graphene matrix for the catalytic oxidation of benzene at room temperature. *Sci. Adv.* **2015**, *1*, e1500462. [[CrossRef](#)]
49. Vilé, G.; Albani, D.; Nachtegaal, M.; Chen, Z.; Dontsova, D.; Antonietti, M.; López, N.; Pérez-Ramírez, J. A Stable Single-Site Palladium Catalyst for Hydrogenations. *Angew. Chem. Int. Ed.* **2015**, *54*, 11265–11269. [[CrossRef](#)]
50. Chen, Z.; Pronkin, S.; Fellinger, T.P.; Kailasam, K.; Vilé, G.; Albani, D.; Krumeich, F.; Leary, R.; Barnard, J.; Thomas, J.M.; et al. Merging Single-Atom-Dispersed Silver and Carbon Nitride to a Joint Electronic System via Copolymerization with Silver Tricyanomethanide. *ACS Nano* **2016**, *10*, 3166–3175. [[CrossRef](#)] [[PubMed](#)]
51. Daelman, N.; Capdevila-Cortada, M.; López, N. Dynamic charge and oxidation state of Pt/CeO₂ single-atom catalysts. *Nat. Mater.* **2019**, *18*, 1215–1221. [[CrossRef](#)] [[PubMed](#)]
52. Kwon, Y.; Kim, T.Y.; Kwon, G.; Yi, J.; Lee, H. Selective Activation of Methane on Single-Atom Catalyst of Rhodium Dispersed on Zirconia for Direct Conversion. *J. Am. Chem. Soc.* **2017**, *139*, 17694–17699. [[CrossRef](#)]
53. Zhao, D.; Chen, Z.; Yang, W.; Liu, S.; Zhang, X.; Yu, Y.; Cheong, W.C.; Zheng, L.; Ren, F.; Ying, G.; et al. MXene (Ti₃C₂) Vacancy-Confined Single-Atom Catalyst for Efficient Functionalization of CO₂. *J. Am. Chem. Soc.* **2019**, *141*, 4086–4093. [[CrossRef](#)]
54. Figueroba, A.; Kovács, G.; Bruix, A.; Neyman, K.M. Towards stable single-atom catalysts: Strong binding of atomically dispersed transition metals on the surface of nanostructured ceria. *Catal. Sci. Technol.* **2016**, *6*, 6806–6813. [[CrossRef](#)]
55. O'Connor, N.J.; Jonayat, A.S.M.; Janik, M.J.; Senftle, T.P. Interaction trends between single metal atoms and oxide supports identified with density functional theory and statistical learning. *Nat. Catal.* **2018**, *1*, 531–539. [[CrossRef](#)]
56. Hou, C.C.; Wang, H.F.; Li, C.; Xu, Q.; Xu, Q.; Xu, Q. From metal-organic frameworks to single/dual-atom and cluster metal catalysts for energy applications. *Energy Environ. Sci.* **2020**, *13*, 1658–1693. [[CrossRef](#)]
57. Liu, D.; Ni, K.; Ye, J.; Xie, J.; Zhu, Y.; Song, L. Tailoring the Structure of Carbon Nanomaterials toward High-End Energy Applications. *Adv. Mater.* **2018**, *30*, 1–13. [[CrossRef](#)]
58. Liu, D.; Ding, S.; Wu, C.; Gan, W.; Wang, C.; Cao, D.; Rehman, Z.U.; Sang, Y.; Chen, S.; Zheng, X.; et al. Synergistic effect of an atomically dual-metal doped catalyst for highly efficient oxygen evolution. *J. Mater. Chem. A* **2018**, *6*, 6840–6846. [[CrossRef](#)]
59. Wang, L.; Chen, M.X.; Yan, Q.Q.; Xu, S.L.; Chu, S.Q.; Chen, P.; Lin, Y.; Liang, H.W. A sulfur-tethering synthesis strategy toward high-loading atomically dispersed noble metal catalysts. *Sci. Adv.* **2019**, *5*, eaax6322. [[CrossRef](#)]
60. Long, X.; Li, Z.; Gao, G.; Sun, P.; Wang, J.; Zhang, B.; Zhong, J.; Jiang, Z.; Li, F. Graphitic phosphorus coordinated single Fe atoms for hydrogenative transformations. *Nat. Commun.* **2020**, *11*, 4074. [[CrossRef](#)] [[PubMed](#)]
61. Ji, Y.; Dong, H.; Liu, C.; Li, Y. Two-dimensional π -conjugated metal-organic nanosheets as single-atom catalysts for the hydrogen evolution reaction. *Nanoscale* **2019**, *11*, 454–458. [[CrossRef](#)] [[PubMed](#)]
62. Bulushev, D.A.; Nishchakova, A.D.; Trubina, S.V.; Stonkus, O.A.; Asanov, I.P.; Okotrub, A.V.; Bulusheva, L.G. Ni-N₄ sites in a single-atom Ni catalyst on N-doped carbon for hydrogen production from formic acid. *J. Catal.* **2021**, *402*, 264–274. [[CrossRef](#)]
63. Cheng, Q.; Yang, L.; Zou, L.; Zou, Z.; Chen, C.; Hu, Z.; Yang, H. Single cobalt atom and N codoped carbon nanofibers as highly durable electrocatalyst for oxygen reduction reaction. *ACS Catal.* **2017**, *7*, 6864–6871. [[CrossRef](#)]
64. Singh, B.; Kumar, S.; Singh, A. Cobalt Single Atom Heterogeneous Catalyst: Method of Preparation, Characterization, Catalysis, and Mechanism. *Cobalt Compd. Appl.* **2019**. [[CrossRef](#)]

65. Hart, A.S.; Kc, C.B.; Gobeze, H.B.; Sequeira, L.R.; D'Souza, F. Porphyrin-sensitized solar cells: Effect of carboxyl anchor group orientation on the cell performance. *ACS Appl. Mater. Interfaces* **2013**, *5*, 5314–5323. [[CrossRef](#)]
66. Eigler, S.; Hirsch, A. Controlled Functionalization of Graphene by Oxo-addends. *Phys. Sci. Rev.* **2019**, *2*, 1–24. [[CrossRef](#)]
67. Liu, J.; Bunes, B.R.; Zang, L.; Wang, C. Supported single-atom catalysts: Synthesis, characterization, properties, and applications. *Environ. Chem. Lett.* **2018**, *16*, 477–505. [[CrossRef](#)]
68. Zhang, Y.; Guo, L.; Tao, L.; Lu, Y.; Wang, S. Defect-Based Single-Atom Electrocatalysts. *Small Methods* **2019**, *3*, 1–17. [[CrossRef](#)]
69. Tang, N.; Cong, Y.; Shang, Q.; Wu, C.; Xu, G.; Wang, X. Coordinatively Unsaturated Al³⁺ Sites Anchored Subnanometric Ruthenium Catalyst for Hydrogenation of Aromatics. *ACS Catal.* **2017**, *7*, 5987–5991. [[CrossRef](#)]
70. Tian, H.; Song, A.; Tian, H.; Liu, J.; Shao, G.; Liu, H.; Wang, G. Single-atom catalysts for high-energy rechargeable batteries. *Chem. Sci.* **2021**, *12*, 7656–7676. [[CrossRef](#)] [[PubMed](#)]
71. Yang, X.F.; Wang, A.; Qiao, B.; Li, J.; Liu, J.; Zhang, T. Single-atom catalysts: A new frontier in heterogeneous catalysis. *Acc. Chem. Res.* **2013**, *46*, 1740–1748. [[CrossRef](#)] [[PubMed](#)]
72. Zhang, H.; Liu, G.; Shi, L.; Ye, J. Single-Atom Catalysts: Emerging Multifunctional Materials in Heterogeneous Catalysis. *Adv. Energy Mater.* **2018**, *8*, 1701343. [[CrossRef](#)]
73. Wei, X.; Yang, X.F.; Wang, A.Q.; Li, L.; Liu, X.Y.; Zhang, T.; Mou, C.Y.; Li, J. Bimetallic Au-Pd alloy catalysts for N₂O decomposition: Effects of surface structures on catalytic activity. *J. Phys. Chem. C* **2012**, *116*, 6222–6232. [[CrossRef](#)]
74. Song, W.; Jansen, A.P.J.; Hensen, E.J.M. A computational study of the influence of the ceria surface termination on the mechanism of CO oxidation of isolated Rh atoms. *Faraday Discuss.* **2013**, *162*, 281. [[CrossRef](#)]
75. Darby, M.T.; Sykes, E.C.H.; Michaelides, A.; Stamatakis, M. Carbon Monoxide Poisoning Resistance and Structural Stability of Single Atom Alloys. *Top. Catal.* **2018**, *61*, 428–438. [[CrossRef](#)]
76. Skriver, H.L.; Rosengaard, N.M. Surface energy and work function of elemental metals. *Phys. Rev. B* **1992**, *46*, 7157–7168. [[CrossRef](#)] [[PubMed](#)]
77. Zhang, N.; Chen, F.; Jin, Y.; Wang, J.; Jin, T.; Kou, B. Alloying effect in silver-based dilute nanoalloy catalysts for oxygen reduction reactions. *J. Catal.* **2020**, *384*, 37–48. [[CrossRef](#)]
78. Fu, Q.; Luo, Y. Catalytic activity of single transition-metal atom doped in Cu(111) surface for heterogeneous hydrogenation. *J. Phys. Chem. C* **2013**, *117*, 14618–14624. [[CrossRef](#)]
79. Yang, K.; Yang, B.; Papanikolaou, K.G.; Darby, M.T.; Stamatakis, M. CO-Induced Aggregation and Segregation of Highly Dilute Alloys: A Density Functional Theory Study. *Phys. Chem. Chem. Phys.* **2019**, *123*, 9128–9138. [[CrossRef](#)]
80. Yang, K.; Yang, B. Surface restructuring of Cu-based single-atom alloy catalysts under reaction conditions: The essential role of adsorbates. *Phys. Chem. Chem. Phys.* **2017**, *19*, 18010–18017. [[CrossRef](#)] [[PubMed](#)]
81. Liu, K.; Zhao, X.; Ren, G.; Yang, T.; Ren, Y.; Lee, A.F.; Su, Y.; Pan, X.; Zhang, J.; Chen, Z.; et al. Strong metal-support interaction promoted scalable production of thermally stable single-atom catalysts. *Nat. Commun.* **2020**, *11*, 1263. [[CrossRef](#)] [[PubMed](#)]
82. Lang, R.; Du, X.; Huang, Y.; Jiang, X.; Zhang, Q.; Guo, Y.; Liu, K.; Qiao, B.; Wang, A.; Zhang, T. Single-Atom Catalysts Based on the Metal-Oxide Interaction. *Chem. Rev.* **2020**, *120*, 11986–12043. [[CrossRef](#)]
83. Wang, Y.; Arandiyani, H.; Scott, J.; Bagheri, A.; Dai, H.; Amal, R. Recent advances in ordered meso/macroporous metal oxides for heterogeneous catalysis: A review. *J. Mater. Chem. A* **2017**, *5*, 8825–8846. [[CrossRef](#)]
84. Védrine, J.C. Importance, features and uses of metal oxide catalysts in heterogeneous catalysis. *Chin. J. Catal.* **2019**, *40*, 1627–1636. [[CrossRef](#)]
85. Xu, H.; Zhang, Z.; Liu, J.; Do-Thanh, C.L.; Chen, H.; Xu, S.; Lin, Q.; Jiao, Y.; Wang, J.; Wang, Y.; et al. Entropy-stabilized single-atom Pd catalysts via high-entropy fluorite oxide supports. *Nat. Commun.* **2020**, *11*, 1–9. [[CrossRef](#)]
86. Lin, J.; Wang, A.; Qiao, B.; Liu, X.; Yang, X.; Wang, X.; Liang, J.; Li, J.; Liu, J.; Zhang, T. Remarkable performance of Ir₁/FeO_x single-atom catalyst in water gas shift reaction. *J. Am. Chem. Soc.* **2013**, *135*, 15314–15317. [[CrossRef](#)] [[PubMed](#)]
87. Fu, J.; Dong, J.; Si, R.; Sun, K.; Zhang, J.; Li, M.; Yu, N.; Zhang, B.; Humphrey, M.G.; Fu, Q.; et al. Synergistic effects for enhanced catalysis in a dual single-atom catalyst. *ACS Catal.* **2021**, *11*, 1952–1961. [[CrossRef](#)]
88. Han, B.; Li, T.; Zhang, J.; Zeng, C.; Matsumoto, H.; Su, Y.; Qiao, B.; Zhang, T. A highly active Rh₁/CeO₂ single-atom catalyst for low-temperature CO oxidation. *Chem. Commun.* **2020**, *56*, 4870–4873. [[CrossRef](#)]
89. Zhou, Y.; Xi, W.; Xie, Z.; You, Z.; Jiang, X.; Han, B.; Lang, R.; Wu, C. High-Loading Pt Single-Atom Catalyst on CeO₂-Modified Diatomite Support. *Chemistry* **2021**, *16*, 2622–2625. [[CrossRef](#)]
90. Luo, R.; Luo, M.; Wang, Z.; Liu, P.; Song, S.; Wang, X.; Chen, M. The atomic origin of nickel-doping-induced catalytic enhancement in MoS₂ for electrochemical hydrogen production. *Nanoscale* **2019**, *11*, 7123–7128. [[CrossRef](#)]
91. Zhang, J.; Xu, X.; Yang, L.; Cheng, D.; Cao, D. Single-Atom Ru Doping Induced Phase Transition of MoS₂ and S Vacancy for Hydrogen Evolution Reaction. *Small Methods* **2019**, *3*, 1–9. [[CrossRef](#)]
92. Wang, Q.; Zhao, Z.L.; Dong, S.; He, D.; Lawrence, M.J.; Han, S.; Cai, C.; Xiang, S.; Rodriguez, P.; Xiang, B.; et al. Design of active nickel single-atom decorated MoS₂ as a pH-universal catalyst for hydrogen evolution reaction. *Nano Energy* **2018**, *53*, 458–467. [[CrossRef](#)]
93. Liu, J.; Shan, J.; Lucci, F.R.; Cao, S.; Sykes, E.C.H.; Flytzani-Stephanopoulos, M. Palladium-gold single atom alloy catalysts for liquid phase selective hydrogenation of 1-hexyne. *Catal. Sci. Technol.* **2017**, *7*, 4276–4284. [[CrossRef](#)]
94. Yang, H.; Shang, L.; Zhang, Q.; Shi, R.; Waterhouse, G.I.N.; Gu, L.; Zhang, T. A universal ligand mediated method for large scale synthesis of transition metal single atom catalysts. *Nat. Commun.* **2019**, *10*, 4585. [[CrossRef](#)] [[PubMed](#)]

95. Zhu, T.; Han, Y.; Liu, S.; Yuan, B.; Liu, Y.; Ma, H. Porous Materials Confining Single Atoms for Catalysis. *Front. Chem.* **2021**, *9*, 1–11. [[CrossRef](#)] [[PubMed](#)]
96. Fei, H.; Dong, J.; Arellano-Jiménez, M.J.; Ye, G.; Dong Kim, N.; Samuel, E.L.G.; Peng, Z.; Zhu, Z.; Qin, F.; Bao, J.; et al. Atomic cobalt on nitrogen-doped graphene for hydrogen generation. *Nat. Commun.* **2015**, *6*, 8668. [[CrossRef](#)]
97. Chabot, V.; Higgins, D.; Yu, A.; Xiao, X.; Chen, Z.; Zhang, J. A review of graphene and graphene oxide sponge: Material synthesis and applications to energy and the environment. *Energy Environ. Sci.* **2014**, *7*, 1564–1596. [[CrossRef](#)]
98. James, S.L.; Adams, C.J.; Bolm, C.; Braga, D.; Collier, P.; Frišćic, T.; Grepioni, F.; Harris, K.D.M.; Hyett, G.; Jones, W.; et al. Mechanochemistry: Opportunities for new and cleaner synthesis. *Chem. Soc. Rev.* **2012**, *41*, 413–447. [[CrossRef](#)]
99. Yi, M.; Shen, Z. A review on mechanical exfoliation for the scalable production of graphene. *J. Mater. Chem. A* **2015**, *3*, 11700–11715. [[CrossRef](#)]
100. Cui, X.; Xiao, J.; Wu, Y.; Du, P.; Si, R.; Yang, H.; Tian, H.; Li, J.; Zhang, W.H.; Deng, D.; et al. A Graphene Composite Material with Single Cobalt Active Sites: A Highly Efficient Counter Electrode for Dye-Sensitized Solar Cells. *Angew. Chem. Int. Ed.* **2016**, *55*, 6708–6712. [[CrossRef](#)]
101. Jiang, X.H.; Zhang, L.S.; Liu, H.Y.; Wu, D.S.; Wu, F.Y.; Tian, L.; Liu, L.L.; Zou, J.P.; Luo, S.L.; Chen, B.B. Silver Single Atom in Carbon Nitride Catalyst for Highly Efficient Photocatalytic Hydrogen Evolution. *Angew. Chem. Int. Ed.* **2020**, *59*, 23112–23116. [[CrossRef](#)]
102. Li, J.C.; Xiao, F.; Zhong, H.; Li, T.; Xu, M.; Ma, L.; Cheng, M.; Liu, D.; Feng, S.; Shi, Q.; et al. Secondary-Atom-Assisted Synthesis of Single Iron Atoms Anchored on N-Doped Carbon Nanowires for Oxygen Reduction Reaction. *ACS Catal.* **2019**, *9*, 5929–5934. [[CrossRef](#)]
103. Zhang, X.; Zhang, S.; Yang, Y.; Wang, L.; Mu, Z.; Zhu, H.; Zhu, X.; Xing, H.; Xia, H.; Huang, B.; et al. A General Method for Transition Metal Single Atoms Anchored on Honeycomb-Like Nitrogen-Doped Carbon Nanosheets. *Adv. Mater.* **2020**, *32*, 1–8. [[CrossRef](#)] [[PubMed](#)]
104. Chen, X.; Fan, K.; Zong, L.; Zhang, Y.; Feng, D.; Hou, M.; Zhang, Q.; Zheng, D.; Chen, Y.; Wang, L. Fe, N-decorated three dimension porous carbonaceous matrix for highly efficient oxygen reduction reaction. *Appl. Surf. Sci.* **2020**, *505*, 144635. [[CrossRef](#)]
105. Zhao, L.; Zhang, Y.; Huang, L.B.; Liu, X.Z.; Zhang, Q.H.; He, C.; Wu, Z.Y.; Zhang, L.J.; Wu, J.; Yang, W.; et al. Cascade anchoring strategy for general mass production of high-loading single-atomic metal-nitrogen catalysts. *Nat. Commun.* **2019**, *10*. [[CrossRef](#)] [[PubMed](#)]
106. Wang, L.; Zhang, J.; Yi, X.; Zheng, A.; Deng, F.; Chen, C.; Ji, Y.; Liu, F.; Meng, X.; Xiao, F.S.; et al. Mesoporous ZSM-5 zeolite-supported ru nanoparticles as highly efficient catalysts for upgrading phenolic biomolecules. *ACS Catal.* **2015**, *5*, 2727–2734. [[CrossRef](#)]
107. Liu, Y.; Li, Z.; Yu, Q.; Chen, Y.; Chai, Z.; Zhao, G.; Liu, S.; Cheong, W.C.; Pan, Y.; Zhang, Q.; et al. A General Strategy for Fabricating Isolated Single Metal Atomic Site Catalysts in γ Zeolite. *J. Am. Chem. Soc.* **2019**, *141*, 9305–9311. [[CrossRef](#)]
108. Sun, Q.; Wang, N.; Zhang, T.; Bai, R.; Mayoral, A.; Zhang, P.; Zhang, Q.; Terasaki, O.; Yu, J. Zeolite-Encaged Single-Atom Rhodium Catalysts: Highly-Efficient Hydrogen Generation and Shape-Selective Tandem Hydrogenation of Nitroarenes. *Angew. Chem. Int. Ed.* **2019**, *58*, 18570–18576. [[CrossRef](#)]
109. Cui, Q.; Qin, G.; Wang, W.; Geethalakshmi, K.R.; Du, A.; Sun, Q. Novel two-dimensional MOF as a promising single-atom electrocatalyst for CO₂ reduction: A theoretical study. *Appl. Surf. Sci.* **2020**, *500*, 143993. [[CrossRef](#)]
110. Li, J.; Huang, H.; Liu, P.; Song, X.; Mei, D.; Tang, Y.; Wang, X.; Zhong, C. Metal-organic framework encapsulated single-atom Pt catalysts for efficient photocatalytic hydrogen evolution. *J. Catal.* **2019**, *375*, 351–360. [[CrossRef](#)]
111. Guo, S.; Zhao, Y.; Wang, C.; Jiang, H.; Jiang, H.; Cheng, G.J.; Cheng, G.J. A Single-Atomic Noble Metal Enclosed Defective MOF via Cryogenic UV Photoreduction for CO Oxidation with Ultrahigh Efficiency and Stability. *ACS Appl. Mater. Interfaces* **2020**, *12*, 26068–26075. [[CrossRef](#)]
112. Zhao, Y.; Zhou, H.; Chen, W.; Tong, Y.; Zhao, C.; Lin, Y.; Jiang, Z.; Zhang, Q.; Xue, Z.; Cheong, W.C.; et al. Two-step carbothermal welding to access atomically dispersed pd1 on three-dimensional zirconia nanonet for direct indole synthesis. *J. Am. Chem. Soc.* **2019**, *141*, 10590–10594. [[CrossRef](#)] [[PubMed](#)]
113. Nongbe, M.C.; Ekou, T.; Ekou, L.; Yao, K.B.; Le Grogne, E.; Felpin, F.X. Biodiesel production from palm oil using sulfonated graphene catalyst. *Renew. Energy* **2017**, *106*, 135–141. [[CrossRef](#)]
114. Sun, S.; Zhang, G.; Gauquelin, N.; Chen, N.; Zhou, J.; Yang, S.; Chen, W.; Meng, X.; Geng, D.; Banis, M.N.; et al. Single-atom catalysis using Pt/graphene achieved through atomic layer deposition. *Sci. Rep.* **2013**, *3*, 1775. [[CrossRef](#)]
115. Qiao, B.; Liu, J.; Wang, Y.G.; Lin, Q.; Liu, X.; Wang, A.; Li, J.; Zhang, T.; Liu, J. Highly Efficient Catalysis of Preferential Oxidation of CO in H₂-Rich Stream by Gold Single-Atom Catalysts. *ACS Catal.* **2015**, *5*, 6249–6254. [[CrossRef](#)]
116. Gu, X.K.; Qiao, B.; Huang, C.Q.; Ding, W.C.; Sun, K.; Zhan, E.; Zhang, T.; Liu, J.; Li, W.X. Supported single Pt₁/Au₁ atoms for methanol steam reforming. *ACS Catal.* **2014**, *4*, 3886–3890. [[CrossRef](#)]
117. Li, P.; Wang, M.; Duan, X.; Zheng, L.; Cheng, X.; Zhang, Y.; Kuang, Y.; Li, Y.; Ma, Q.; Feng, Z. Boosting oxygen evolution of single-atomic ruthenium through electronic coupling with cobalt-iron layered double hydroxides. *Nat. Commun.* **2019**, *10*, 1–11. [[CrossRef](#)]
118. Xia, X.; Wang, Y.; Ruditskiy, A.; Xia, Y. 25th anniversary article: Galvanic replacement: A simple and versatile route to hollow nanostructures with tunable and well-controlled properties. *Adv. Mater.* **2013**, *25*, 6313–6333. [[CrossRef](#)]

119. Boucher, M.B.; Zugic, B.; Cladaras, G.; Kammert, J.; Marcinkowski, M.D.; Lawton, T.J.; Sykes, E.C.H.; Flytzani-Stephanopoulos, M. Single atom alloy surface analogs in Pd_{0.18}Cu₁₅ nanoparticles for selective hydrogenation reactions. *Phys. Chem. Chem. Phys.* **2013**, *15*, 12187–12196. [[CrossRef](#)]
120. Shan, J.; Liu, J.; Li, M.; Lustig, S.; Lee, S.; Flytzani-Stephanopoulos, M. NiCu single atom alloys catalyze the C–H bond activation in the selective non-oxidative ethanol dehydrogenation reaction. *Appl. Catal. B Environ.* **2018**, *226*, 534–543. [[CrossRef](#)]
121. Marcinkowski, M.D.; Darby, M.T.; Liu, J.; Wimble, J.M.; Lucci, F.R.; Lee, S.; Michaelides, A.; Flytzani-Stephanopoulos, M.; Stamatakis, M.; Sykes, E.C.H. Catalysts for efficient C–H activation. *Nat. Chem.* **2018**, *10*, 325–332. [[CrossRef](#)]
122. Lucci, F.R.; Liu, J.; Marcinkowski, M.D.; Yang, M.; Allard, L.F.; Flytzani-Stephanopoulos, M.; Sykes, E.C.H. Selective hydrogenation of 1,3-butadiene on platinum–copper alloys at the single-atom limit. *Nat. Commun.* **2015**, *6*, 8550. [[CrossRef](#)]
123. Mao, J.; Yin, J.; Pei, J.; Wang, D.; Li, Y. Single atom alloy: An emerging atomic site material for catalytic applications. *Nano Today* **2020**, *34*, 100917. [[CrossRef](#)]
124. Sun, G.; Zhao, Z.J.; Mu, R.; Zha, S.; Li, L.; Chen, S.; Zang, K.; Luo, J.; Li, Z.; Purdy, S.C.; et al. Breaking the scaling relationship via thermally stable Pt/Cu single atom alloys for catalytic dehydrogenation. *Nat. Commun.* **2018**, *9*, 4454. [[CrossRef](#)]
125. Aich, P.; Wei, H.; Basan, B.; Kropf, A.J.; Schweitzer, N.M.; Marshall, C.L.; Miller, J.T.; Meyer, R. Single-atom alloy Pd–Ag catalyst for selective hydrogenation of acrolein. *J. Phys. Chem. C* **2015**, *119*, 18140–18148. [[CrossRef](#)]
126. Kim, J.; Roh, C.W.; Sahoo, S.K.; Yang, S.; Bae, J.; Han, J.W.; Lee, H. Highly Durable Platinum Single-Atom Alloy Catalyst for Electrochemical Reactions. *Adv. Energy Mater.* **2018**, *8*, 1–8. [[CrossRef](#)]
127. Baptista, A.; Silva, F.; Porteiro, J.; Míguez, J.; Pinto, G. Sputtering physical vapour deposition (PVD) coatings: A critical review on process improvement and market trend demands. *Coatings* **2018**, *8*, 402. [[CrossRef](#)]
128. Kyriakou, G.; Boucher, M.B.; Jewell, A.D.; Lewis, E.A.; Lawton, T.J.; Baber, A.E.; Tierney, H.L.; Flytzani-Stephanopoulos, M.; Sykes, E.C.H. Isolated metal atom geometries as a strategy for selective heterogeneous hydrogenations. *Science (80-)* **2012**, *335*, 1209–1212. [[CrossRef](#)]
129. Lucci, F.R.; Darby, M.T.; Mattera, M.F.G.; Ivimey, C.J.; Therrien, A.J.; Michaelides, A.; Stamatakis, M.; Sykes, E.C.H. Controlling hydrogen activation, spillover, and desorption with Pd–Au single-atom alloys. *J. Phys. Chem. Lett.* **2016**, *7*, 480–485. [[CrossRef](#)] [[PubMed](#)]
130. Hannagan, R.T.; Giannakakis, G.; Réocreux, R.; Schumann, J.; Finzel, J.; Wang, Y.; Michaelides, A.; Deshlahra, P.; Christopher, P.; Flytzani-Stephanopoulos, M. First-principles design of a single-atom–alloy propane dehydrogenation catalyst. *Science (80-)* **2021**, *372*, 1444–1447. [[CrossRef](#)]
131. Wang, H.; Luo, Q.; Liu, W.; Lin, Y.; Guan, Q.; Zheng, X.; Pan, H.; Zhu, J.; Sun, Z.; Wei, S.; et al. Quasi Pd₁Ni single-atom surface alloy catalyst enables hydrogenation of nitriles to secondary amines. *Nat. Commun.* **2019**, *10*, 4998. [[CrossRef](#)]
132. Pei, G.X.; Liu, X.Y.; Wang, A.; Li, L.; Huang, Y.; Zhang, T.; Lee, J.W.; Jang, B.W.L.; Mou, C.-Y. Promotional effect of Pd single atoms on Au nanoparticles supported on silica for the selective hydrogenation of acetylene in excess ethylene. *New J. Chem.* **2014**, *38*, 2043–2051. [[CrossRef](#)]
133. Trimpalis, A.; Giannakakis, G.; Cao, S.; Flytzani-Stephanopoulos, M. NiAu single atom alloys for the selective oxidation of methacrolein with methanol to methyl methacrylate. *Catalysis Today*. **2020**, *355*, 804–814. [[CrossRef](#)]
134. Yao, Y.; Hu, S.; Chen, W.; Huang, Z.-Q.; Wei, W.; Yao, T.; Liu, R.; Zang, K.; Wang, X.; Wu, G. Engineering the electronic structure of single atom Ru sites via compressive strain boosts acidic water oxidation electrocatalysis. *Nat. Catal.* **2019**, *2*, 304–313. [[CrossRef](#)]
135. Wang, J.; Li, Z.; Wu, Y.; Li, Y. Fabrication of single-atom catalysts with precise structure and high metal loading. *Adv. Mater.* **2018**, *30*, 1801649. [[CrossRef](#)] [[PubMed](#)]
136. Wu, Y. Sophisticated construction of Au islands on Pt–Ni: An ideal trimetallic nanoframe catalyst. In *Controlled Synthesis of Pt–Ni Bimetallic Catalysts and Study of Their Catalytic Properties*; Springer: Berlin/Heidelberg, Germany, 2016; pp. 93–111.
137. Balajii, M.; Niju, S. Biochar-derived heterogeneous catalysts for biodiesel production. *Environ. Chem. Lett.* **2019**, *17*, 1447–1469. [[CrossRef](#)]
138. Bhatia, S.K.; Gurav, R.; Choi, T.-R.R.; Kim, H.J.; Yang, S.-Y.Y.; Song, H.-S.S.; Park, J.Y.; Park, Y.-L.L.; Han, Y.-H.H.; Choi, Y.-K.K.; et al. Conversion of waste cooking oil into biodiesel using heterogenous catalyst derived from cork biochar. *Bioresour. Technol.* **2020**, *302*, 122872. [[CrossRef](#)] [[PubMed](#)]
139. Mortensen, P.M.; Grunwaldt, J.-D.; Jensen, P.A.; Knudsen, K.G.; Jensen, A.D. A review of catalytic upgrading of bio-oil to engine fuels. *Appl. Catal. A Gen.* **2011**, *407*, 1–19. [[CrossRef](#)]
140. Pérez-Mayoral, E.; Matos, I.; Bernardo, M.; Ventura, M.; Fonseca, I.M. Carbon-based materials for the development of highly dispersed metal catalysts: Towards highly performant catalysts for fine chemical synthesis. *Catalysts* **2020**, *10*, 1407. [[CrossRef](#)]
141. Li, J.; Chen, S.; Yang, N.; Deng, M.; Ibraheem, S.; Deng, J.; Li, J.; Li, L.; Wei, Z. Ultrahigh-loading zinc single-atom catalyst for highly efficient oxygen reduction in both acidic and alkaline media. *Angew. Chem. Int. Ed.* **2019**, *58*, 7035–7039. [[CrossRef](#)]
142. Yin, P.; Yao, T.; Wu, Y.; Zheng, L.; Lin, Y.; Liu, W.; Ju, H.; Zhu, J.; Hong, X.; Deng, Z. Single cobalt atoms with precise N-coordination as superior oxygen reduction reaction catalysts. *Angew. Chem.* **2016**, *128*, 10958–10963. [[CrossRef](#)]
143. Zhao, C.; Dai, X.; Yao, T.; Chen, W.; Wang, X.; Wang, J.; Yang, J.; Wei, S.; Wu, Y.; Li, Y. Ionic Exchange of Metal–Organic Frameworks to Access Single Nickel Sites for Efficient Electroreduction of CO₂. *J. Am. Chem. Soc.* **2017**, *139*, 8078–8081. [[CrossRef](#)]
144. Gan, T.; Liu, Y.; He, Q.; Zhang, H.; He, X.; Ji, H. Facile synthesis of kilogram-scale Co-alloyed Pt single-atom catalysts via ball milling for hydrodeoxygenation of 5-hydroxymethylfurfural. *ACS Sustain. Chem. Eng.* **2020**, *8*, 8692–8699. [[CrossRef](#)]

145. Gan, T.; He, Q.; Zhang, H.; Xiao, H.; Liu, Y.; Zhang, Y.; He, X.; Ji, H. Unveiling the kilogram-scale gold single-atom catalysts via ball milling for preferential oxidation of CO in excess hydrogen. *Chem. Eng. J.* **2020**, *389*, 124490. [[CrossRef](#)]
146. Liu, G.; Robertson, A.W.; Li, M.M.J.; Kuo, W.C.H.; Darby, M.T.; Muhieddine, M.H.; Lin, Y.C.; Suenaga, K.; Stamatakis, M.; Warner, J.H.; et al. MoS₂ monolayer catalyst doped with isolated Co atoms for the hydrodeoxygenation reaction. *Nat. Chem.* **2017**, *9*, 810–816. [[CrossRef](#)]
147. Cao, W.; Luo, W.; Ge, H.; Su, Y.; Wang, A.; Zhang, T. UiO-66 derived Ru/ZrO₂@C as a highly stable catalyst for hydrogenation of levulinic acid to γ -valerolactone. *Green Chem.* **2017**, *19*, 2201–2211. [[CrossRef](#)]
148. Bhattacharjee, S.; Lende, A.B.; Anbalagan, A.K.; Lee, C.-H.; Tan, C.-S. Development and Characterization of a One-Pot Synthesized Fe–Au–Pd Surface Alloy Catalyst for Highly Selective Conversion of Castor Oil to Octadecane via Hydrodeoxygenation. *Energy Fuels* **2021**, *35*, 16637–16652. [[CrossRef](#)]
149. Akri, M.; El Kasmi, A.; Batiot-Dupeyrat, C.; Qiao, B. Highly active and carbon-resistant nickel single-atom catalysts for methane dry reforming. *Catalysts* **2020**, *10*, 630. [[CrossRef](#)]
150. Wang, K.; Jiang, L.; Xin, T.; Li, Y.; Wu, X.; Zhang, G. Single-atom V–N charge-transfer bridge on ultrathin carbon nitride for efficient photocatalytic H₂ production and formaldehyde oxidation under visible light. *Chem. Eng. J.* **2022**, *429*, 132229. [[CrossRef](#)]
151. Jin, X.; Wang, R.; Zhang, L.; Si, R.; Shen, M.; Wang, M.; Tian, J.; Shi, J. Electron Configuration Modulation of Nickel Single Atoms for Elevated Photocatalytic Hydrogen Evolution. *Angew. Chem. Int. Ed.* **2020**, *59*, 6827–6831. [[CrossRef](#)]
152. Zhang, L.; Long, R.; Zhang, Y.; Duan, D.; Xiong, Y.; Zhang, Y.; Bi, Y. Direct Observation of Dynamic Bond Evolution in Single-Atom Pt/C₃N₄ Catalysts. *Angew. Chem. Int. Ed.* **2020**, *59*, 6224–6229. [[CrossRef](#)]
153. Zhou, P.; Lv, F.; Li, N.; Zhang, Y.; Mu, Z.; Tang, Y.; Lai, J.; Chao, Y.; Luo, M.; Lin, F.; et al. Strengthening reactive metal-support interaction to stabilize high-density Pt single atoms on electron-deficient g-C₃N₄ for boosting photocatalytic H₂ production. *Nano Energy* **2019**, *56*, 127–137. [[CrossRef](#)]
154. Trofimovaite, R.; Parlett, C.M.A.; Kumar, S.; Frattini, L.; Isaacs, M.A.; Wilson, K.; Olivi, L.; Coulson, B.; Debgupta, J.; Douthwaite, R.E.; et al. Single atom Cu(I) promoted mesoporous titania for photocatalytic Methyl Orange depollution and H₂ production. *Appl. Catal. B Environ.* **2018**, *232*, 501–511. [[CrossRef](#)]
155. Liang, J.X.; Lin, J.; Liu, J.; Wang, X.; Zhang, T.; Li, J. Dual Metal Active Sites in an Ir₁/FeO_x Single-Atom Catalyst: A Redox Mechanism for the Water-Gas Shift Reaction. *Angew. Chem. Int. Ed.* **2020**, *59*, 12868–12875. [[CrossRef](#)]
156. Li, Q.; Ma, Z.; Sa, R.; Adidharma, H.; Gasem, K.A.M.; Russell, A.G.; Fan, M.; Wu, K. Computation-predicted, stable, and inexpensive single-atom nanocatalyst Pt@Mo₂C—an important advanced material for H₂ production. *J. Mater. Chem. A* **2017**, *5*, 14658–14672. [[CrossRef](#)]
157. He, Q.; Liu, D.; Lee, J.H.; Liu, Y.; Xie, Z.; Hwang, S.; Kattel, S.; Song, L.; Chen, J.G. Electrochemical Conversion of CO₂ to Syngas with Controllable CO/H₂ Ratios over Co and Ni Single-Atom Catalysts. *Angew. Chem. Int. Ed.* **2020**, *59*, 3033–3037. [[CrossRef](#)]
158. Pei, G.X.; Liu, X.Y.; Yang, X.; Zhang, L.; Wang, A.; Li, L.; Wang, H.; Wang, X.; Zhang, T. Performance of Cu-Alloyed Pd Single-Atom Catalyst for Semihydrogenation of Acetylene under Simulated Front-End Conditions. *ACS Catal.* **2017**, *7*, 1491–1500. [[CrossRef](#)]
159. Lu, Y.; Zhang, Z.; Wang, H.; Wang, Y. Toward efficient single-atom catalysts for renewable fuels and chemicals production from biomass and CO₂. *Appl. Catal. B Environ.* **2021**, *292*, 120162. [[CrossRef](#)]
160. Zhao, S.; Wen, Y.; Liu, X.; Pen, X.; Lü, F.; Gao, F.; Xie, X.; Du, C.; Yi, H.; Kang, D.; et al. Formation of active oxygen species on single-atom Pt catalyst and promoted catalytic oxidation of toluene. *Nano Res.* **2020**, *13*, 1544–1551. [[CrossRef](#)]
161. Gu, H.; Liu, X.; Liu, X.; Ling, C.; Wei, K.; Zhan, G.; Guo, Y.; Zhang, L. Adjacent single-atom irons boosting molecular oxygen activation on MnO₂. *Nat. Commun.* **2021**, *12*, 5422. [[CrossRef](#)]
162. Liu, J.; Jiao, M.; Mei, B.; Tong, Y.; Li, Y.; Ruan, M.; Song, P.; Sun, G.; Jiang, L.; Wang, Y.; et al. Carbon-Supported Divacancy-Anchored Platinum Single-Atom Electrocatalysts with Superhigh Pt Utilization for the Oxygen Reduction Reaction. *Angew. Chem.* **2019**, *131*, 1175–1179. [[CrossRef](#)]
163. Zhang, X.; Lei, J.; Wu, D.; Zhao, X.; Jing, Y.; Zhou, Z. A Ti-anchored Ti₂CO₂ monolayer (MXene) as a single-atom catalyst for CO oxidation. *J. Mater. Chem. A* **2016**, *4*, 4871–4876. [[CrossRef](#)]
164. Chen, Y.; Ji, S.; Chen, C.; Peng, Q.; Wang, D.; Li, Y. Single-Atom Catalysts: Synthetic Strategies and Electrochemical Applications. *Joule* **2018**, *2*, 1242–1264. [[CrossRef](#)]
165. Xin, Y.; Zhang, N.; Lv, Y.; Wang, J.; Li, Q.; Zhang, Z. From nanoparticles to single atoms for Pt/CeO₂: Synthetic strategies, characterizations and applications. *J. Rare Earths* **2020**, *38*, 850–862. [[CrossRef](#)]
166. Rong, X.; Wang, H.J.; Lu, X.L.; Si, R.; Lu, T.B. Controlled Synthesis of a Vacancy-Defect Single-Atom Catalyst for Boosting CO₂ Electroreduction. *Angew. Chem. Int. Ed.* **2020**, *59*, 1961–1965. [[CrossRef](#)] [[PubMed](#)]
167. Kunwar, D.; Zhou, S.; Delariva, A.; Peterson, E.J.; Xiong, H.; Pereira-Hernández, X.I.; Purdy, S.C.; Ter Veen, R.; Brongersma, H.H.; Miller, J.T.; et al. Stabilizing High Metal Loadings of Thermally Stable Platinum Single Atoms on an Industrial Catalyst Support. *ACS Catal.* **2019**, *9*, 3978–3990. [[CrossRef](#)]